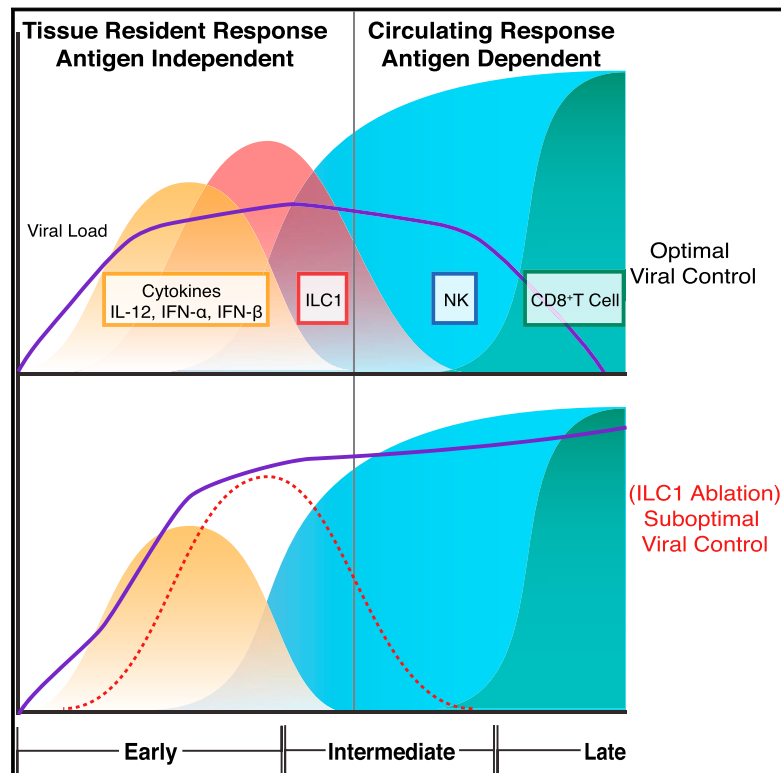


ILC1 Confer Early Host Protection at Initial Sites of Viral Infection

Graphical Abstract



Authors

Orr-EI Weizman, Nicholas M. Adams, Iona S. Schuster, ..., Christina S. Leslie, Joseph C. Sun, Timothy E. O'Sullivan

Correspondence

sunj@mskcc.org (J.C.S.),
tosullivan@mednet.ucla.edu (T.E.O.)

In Brief

Innate lymphoid cells have a non-redundant role as initial responders to viral infections.

Highlights

- ILC1 represent the major early source of IFN- γ in virally infected tissues
- ILC1-derived IFN- γ limits early MCMV replication in primary infected tissues
- Crosstalk between cDC1 and ILC1 populations mediate initial local control of virus
- ILC1 display enhanced responsiveness to IL-12 compared to other lymphocytes



ILC1 Confer Early Host Protection at Initial Sites of Viral Infection

Orr-El Weizman,¹ Nicholas M. Adams,¹ Iona S. Schuster,^{2,3} Chirag Krishna,⁴ Yuri Pritykin,⁴ Colleen Lau,¹ Mariapia A. Degli-Esposti,^{2,3} Christina S. Leslie,⁴ Joseph C. Sun,^{1,5,*} and Timothy E. O'Sullivan^{1,6,7,*}

¹Immunology Program, Memorial Sloan Kettering Cancer Center, New York, NY 10065, USA

²Immunology and Virology Program, Centre for Ophthalmology and Visual Science, The University of Western Australia, Crawley, WA, Australia

³Centre for Experimental Immunology, Lions Eye Institute, Nedlands, WA, Australia

⁴Computational and Systems Biology Program, Memorial Sloan Kettering Cancer Center, New York, NY 10065, USA

⁵Department of Immunology and Microbial Pathogenesis, Weill Cornell Medical College, New York, NY 10065, USA

⁶Present address: Department of Microbiology, Immunology, and Molecular Genetics, David Geffen School of Medicine at UCLA, Los Angeles, CA 90095, USA

⁷Lead Contact

*Correspondence: sunj@mskcc.org (J.C.S.), tosullivan@mednet.ucla.edu (T.E.O.)

<https://doi.org/10.1016/j.cell.2017.09.052>

SUMMARY

Infection is restrained by the concerted activation of tissue-resident and circulating immune cells. Whether tissue-resident lymphocytes confer early antiviral immunity at local sites of primary infection prior to the initiation of circulating responses is not well understood. Furthermore, the kinetics of initial antiviral responses at sites of infection remain unclear. Here, we show that tissue-resident type 1 innate lymphoid cells (ILC1) serve an essential early role in host immunity through rapid production of interferon (IFN)- γ following viral infection. Ablation of *Zfp683*-dependent liver ILC1 lead to increased viral load in the presence of intact adaptive and innate immune cells critical for mouse cytomegalovirus (MCMV) clearance. Swift production of interleukin (IL)-12 by tissue-resident XCR1⁺ conventional dendritic cells (cDC1) promoted ILC1 production of IFN- γ in a STAT4-dependent manner to limit early viral burden. Thus, ILC1 contribute an essential role in viral immunosurveillance at sites of initial infection in response to local cDC1-derived proinflammatory cytokines.

INTRODUCTION

A major role of the host immune system is to recognize a diverse array of “foreign” pathogens and direct effective responses to suppress pathogen replication and distribution. To achieve this, protective immunity involves the coordinated response of both innate and adaptive immune systems. The innate immune system recognizes pathogens through germline-encoded pattern recognition receptors that interact with conserved motifs shared among many pathogens, whereas the adaptive immune system generates antigen receptor diversity by somatic

recombination to provide an immense pool of unique lymphocytes with a higher degree of molecular specificity to a diverse range of pathogens (Goldrath and Bevan, 1999; Iwasaki and Medzhitov, 2004). Although the generation of adaptive lymphocyte clones in higher vertebrates confers the host with enhanced discrimination of pathogens and protective immunological memory, the trade-off between exceptionally high molecular specificity is the tremendously low precursor frequency of individual adaptive lymphocyte clones (Goldrath and Bevan, 1999; Jenkins et al., 2010). Because of their relative rarity in relation to other immune cells, a given pathogen-specific adaptive lymphocyte (such as a naive CD8⁺ T cell) cannot be present at potential sites of infection at all times to encounter antigen. Instead, this naive T cell will constantly recirculate through the blood and lymph until it recognizes its cognate antigen on antigen-presenting cells that migrate from the initial site of infection to draining lymph nodes (von Andrian and Mackay, 2000). Antigen encounter then leads to clonal proliferation of T cells and effector responses that are then recruited back to the initial site of infection to suppress pathogen replication and spread (von Andrian and Mackay, 2000). Although circulating effector T cells can contribute to host protection at tissue sites through generation of antigen-specific responses, the relative speed of the adaptive immune response is slow (requiring ~1 week for maximum effector T cell numbers) compared to the rate of replication for certain pathogens, and by itself, would result in defective host protection (Brown et al., 2001; Goldrath and Bevan, 1999).

In recent years, it has become evident that a complete immune response requires an evolutionary division of labor between tissue-resident and circulating responses. Innate immune cells, such as macrophages and dendritic cells (DCs), generally reside in peripheral tissues and can recognize pathogens through the expression of toll-like receptors (TLRs) to produce a wide-variety of effector molecules that can directly or indirectly limit early pathogen replication at the site of infection (Iwasaki and Medzhitov, 2004). However, the recently described diversity and relative abundance of tissue-resident lymphocytes

in peripheral organs suggests that early myeloid responses alone cannot efficiently restrain pathogen replication in infected tissues before initiation of antigen-specific T cell responses (Fan and Rudensky, 2016). Indeed, tissue-resident lymphocytes, such as innate lymphoid cells (ILCs) and “unconventional” T cells (invariant natural killer T cells [iNKT], $\gamma\delta$ T cells, and mucosal-associated invariant T cells [MAIT]) have been shown to have critical roles during pathogen challenge (Artis and Spits, 2015; Godfrey et al., 2015; Serafini et al., 2015). Unconventional T cells generally express a limited T cell receptor (TCR) repertoire and can be activated by microbial products in the context of nonclassical MHC molecules to rapidly respond within hours to days in infected tissues (Fan and Rudensky, 2016; Godfrey et al., 2015). In contrast, tissue-resident ILCs do not express rearranged antigen receptors, but instead express germline-encoded activating receptors to sense host myeloid and parenchymal cell signals produced following local injury, inflammation, or pathogen infection to rapidly produce proinflammatory and regulatory cytokines (Artis and Spits, 2015; Serafini et al., 2015).

Although tissue-resident unconventional T cell responses have been observed to precede circulating responses during primary microbial infection in an antigen-specific manner (Godfrey et al., 2015), whether this process similarly occurs during viral infection is unclear. Because viruses use host machinery to assemble infectious particles, virally encoded nucleic acid motifs are recognized by certain TLRs expressed by tissue-resident myeloid cells (Iwasaki and Medzhitov, 2004). Following primary viral infection, virus-specific effector T cells can give rise to tissue-resident memory T cells (T_{RM}) that rapidly and robustly respond to secondary viral infection (Schenkel and Masopust, 2014). During mouse cytomegalovirus (MCMV) infection, circulating NK cells and unconventional T cells can produce the antiviral cytokine interferon ($IFN-\gamma$) in an antigen-independent “innate” manner in response to proinflammatory cytokines produced by tissue-resident myeloid cells (Ninomiya et al., 2000; Sun et al., 2012; Wesley et al., 2008). However, whether tissue-resident lymphocytes confer immediate host protection at initial sites of viral infection prior to the initiation of circulating responses in naive hosts is not known. Furthermore, the overall cellular composition and kinetics of the primary antiviral response at the initial site of viral infection in naive hosts remain to be elucidated.

In this study, we show that whereas adaptive immunity is not required for early viral control in naive hosts, ILC responses are critical. Specifically, tissue-resident ILC1 rapidly produced $IFN-\gamma$ at sites of primary viral infection before other known innate and adaptive lymphocytes. Genetic ablation of liver ILC1 lead to increased MCMV load, even in the presence of intact NK cell responses. Crosstalk between tissue-resident $XCR1^+$ dendritic cells and ILC1 via interleukin (IL)-12 was critical to limit early viral burden at primary sites of infection. ILC1 displayed greater sensitivity to IL-12 than any other $IFN-\gamma$ producing lymphocyte, explained by greater *Il12rb1* and *Ifng* transcripts at steady state. Thus, our study reveals a physiologic role for tissue-resident ILC1 in viral immunosurveillance at initial sites of infection where they represent the naive host's first line of defense.

RESULTS

Innate Lymphocytes Are Required to Suppress Early Viral Replication at Initial Sites of Infection

Previous studies have shown that MCMV infection leads to activation of splenic and liver $IFN-\gamma$ producing innate and adaptive lymphocytes as early as 36 hr post-infection (PI) (Lanier, 2008; Nguyen et al., 2002; Ninomiya et al., 2000; Wesley et al., 2008). However, whether resident lymphocyte responses restrain viral replication at the initial site of infection before viral dissemination in naive hosts, or activation of circulating lymphocytes is unknown. To determine whether lymphocytes can confer early host viral protection in the peritoneal cavity (PC), the site of injection, we infected immune-sufficient wild-type (WT), adaptive lymphocyte-deficient *Rag2*^{-/-}, or adaptive lymphocyte and ILC-deficient *Rag2*^{-/-} \times *Il2rg*^{-/-} mice with MCMV by intraperitoneal (i.p.) injection and analyzed viral titers in the PC at 36 hr PI. Although early control of MCMV replication was not dependent on adaptive lymphocytes, viral titers were increased significantly in *Rag2*^{-/-} \times *Il2rg*^{-/-} mice compared to both *Rag2*^{-/-} and WT mice (Figure 1A), suggesting that ILCs mediate early host antiviral defense in the PC of naive mice.

NK cells are known to confer host resistance to MCMV through production of $IFN-\gamma$ and killing of virally infected cells (Lanier, 2008); therefore, we treated *Rag2*^{-/-} mice with either α -NK1.1 or α - $IFN-\gamma$ antibodies prior to infection. Analysis of PC viral titers at 36 hr PI revealed that both NK1.1-depleted and $IFN-\gamma$ -neutralized groups had heightened levels of viral replication in a similar manner to total lymphocyte-deficient mice (Figure 1B), suggesting that $IFN-\gamma$ and NK1.1⁺ cells in the PC are required for early host antiviral resistance, similar to previous results found in the spleen and liver at 48 hr PI (Loh et al., 2005).

Because the relative percentage and composition of tissue-resident lymphocytes is unique to each organ (Fan and Rudensky, 2016), and a major site of viral dissemination and replication of both MCMV and human cytomegalovirus (HCMV) is the host liver (Paya et al., 1989; Salazar-Mather et al., 1998), we tested whether ILCs could also confer early host protection when MCMV was delivered directly to this organ using a hydrodynamic (h.d.) injection model. Similar to results obtained with i.p. infection, h.d. MCMV infection showed increased viral titers in *Rag2*^{-/-} \times *Il2rg*^{-/-} mice compared to both *Rag2*^{-/-} and WT mice (Figure 1C). Protection was dependent on both NK1.1⁺ cells and $IFN-\gamma$ (Figure 1D), suggesting that early NK1.1⁺ ILC-mediated control of MCMV can occur at an initial site of viral replication in an $IFN-\gamma$ -dependent manner that is not limited to discrete tissue microenvironments. Because initial viral entry predominantly occurs at mucosal surfaces (i.e., lung, skin, mouth) (Iwasaki and Medzhitov, 2015), we also tested whether lung resident NK1.1⁺ ILCs could confer host protection following intranasal (i.n.) administration of the mouse respiratory virus, Sendai virus (SeV). Consistent with MCMV infection, higher SeV titers were detected in *Rag2*^{-/-} \times *Il2rg*^{-/-} mice compared to both *Rag2*^{-/-} and WT mice (Figure 1E), and α -NK1.1-treated *Rag2*^{-/-} mice displayed heightened viral burden similar to total lymphocyte-deficient mice (Figure 1F). Together, these results suggest that NK1.1⁺ ILCs confer early viral host protection at initial sites of infection in both barrier and non-barrier tissues.

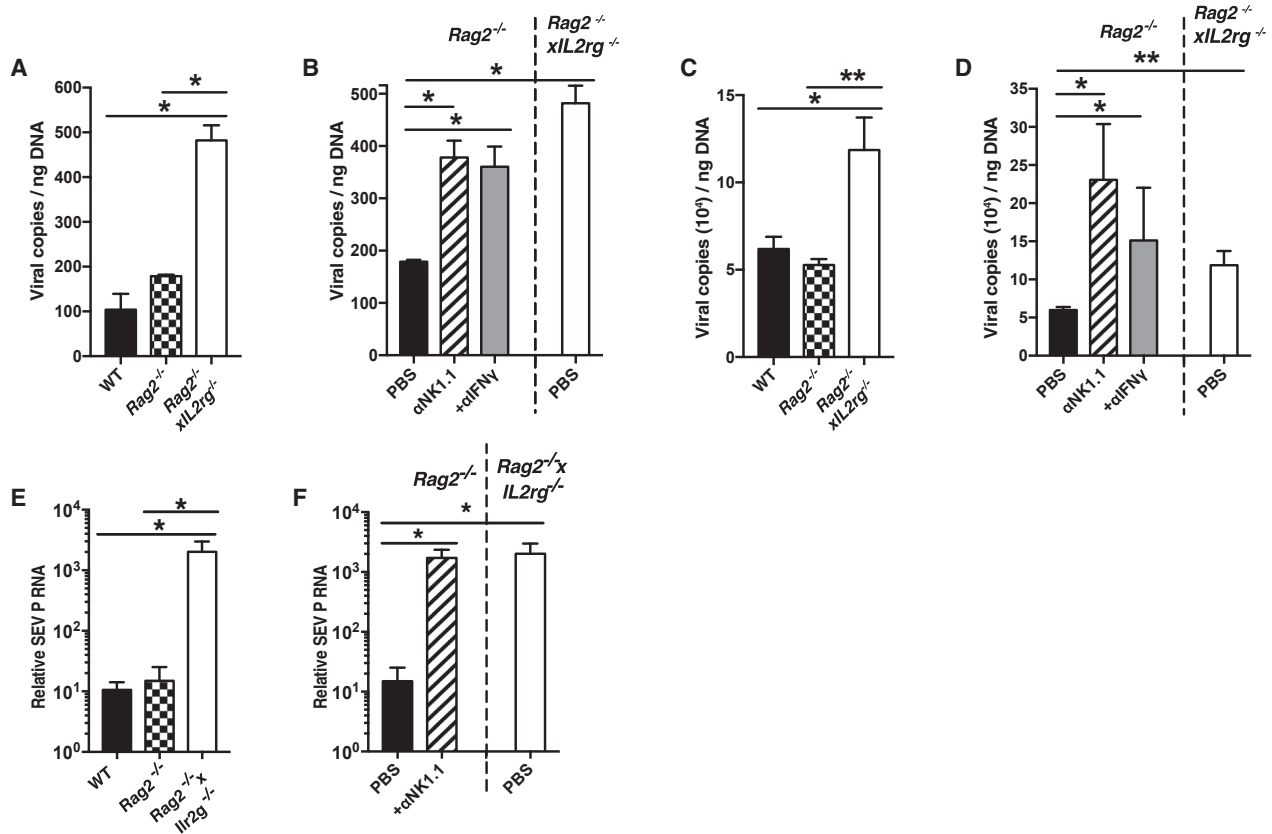


Figure 1. Group 1 ILCs and IFN- γ Confer Early Viral Control at Local Sites of Infection

(A and B) WT, *Rag2*^{-/-}, and *Rag2*^{-/-} *IL2rg*^{-/-} mice (A) and *Rag2*^{-/-} mice (B) treated with PBS, α -NK1.1, or α -IFN- γ were infected with MCMV intraperitoneally (i.p.). Viral titers were measured in the peritoneal cavity (PC) at 36 hr post-infection (PI).

(C and D) WT, *Rag2*^{-/-}, and *Rag2*^{-/-} *IL2rg*^{-/-} mice (C) and *Rag2*^{-/-} mice (D) treated with PBS, α -NK1.1, or α -IFN- γ were infected with MCMV hydrodynamically (h.d.). Viral titers were measured in the liver at 36 hr PI.

(E and F) WT, *Rag2*^{-/-}, and *Rag2*^{-/-} *IL2rg*^{-/-} mice (E) and *Rag2*^{-/-} mice (F) treated with PBS or α -NK1.1 were infected with SeV intranasally (i.n.). Viral load was measured in the lung at 48 hr post-infection (PI) by real-time qPCR. Data are representative of 2 independent experiments of 4–6 mice per group. Samples were compared using an unpaired, two-tailed Student's *t* test, and data are presented as the mean \pm SEM (**p* < 0.05, ***p* < 0.01).

The Peritoneal Cavity Consists of Phenotypically and Functionally Heterogeneous Group 1 ILCs

Recently it has been appreciated that NK1.1⁺ ILCs consist of a diverse family of group 1 ILCs including mature NK cells, immature NK cells, and tissue-resident ILC1 (O'Sullivan et al., 2015). However, the phenotypic and functional heterogeneity of group 1 ILCs in the PC remained unknown. Gating on lin⁻Tbet⁺NK1.1⁺NKp46⁺ cells, we found that the PC consisted of two main subsets of CD49b⁺Eomes⁺ and CD49b⁻Eomes⁻ cells, similar to NK cells and tissue-resident ILC1 described in the liver (Figure 2A) (O'Sullivan et al., 2015). PC CD49b⁺Eomes⁺ cells were dependent on the transcription factors T-bet and Eomes for their development in a cell-intrinsic manner (Figures S1A and S1B) and were derived from the circulation in parabiotic mice (Figures 2B and 2C), consistent with a mature NK cell phenotype in other organs (Figures S1A and S1B). Conversely, PC CD49b⁻Eomes⁻ cells required T-bet, but not Eomes for their development (Figures S1A and S1B) and remained tissue-resident in parabiotic mice (Figures 2B and 2C), consistent with an ILC1 phenotype observed in other peripheral organs (Figures S1A and S1B). Un-

expectedly, PC and splenic CD49b⁻Eomes⁻ cells did not require *Nfil3* for their development (Figure S1C), suggesting these cells may use a different developmental pathway than reported for other ILCs (Geiger et al., 2014).

Using *Eomes*-GFP reporter mice, we then compared the gene expression profile of PC CD49b⁻Eomes⁻ cells with ILC1 and NK cells across multiple organs. Unbiased analysis revealed that genes more highly expressed in ILC1 than in NK cells across tissues examined also had much higher expression in PC CD49b⁻Eomes⁻ cells than in PC CD49b⁺Eomes⁺ NK cells, and conversely, genes more highly expressed in NK cells than in ILC1 also had much higher expression in PC CD49b⁺Eomes⁺ NK cells (Figure S2A). These results are supportive of PC CD49b⁻Eomes⁻ cells being ILC1. Using all available samples, we identified a 713-gene ILC1 versus NK signature across tissues, consisting of 407 genes more highly expressed in ILC1 and 306 genes more highly expressed in NK cells (Figures 2D and S2B). This signature gene set aligned well with, and substantially extended, the previously identified ILC and NK signature genes (Figure S2C) (Robinette et al., 2015). The signature set

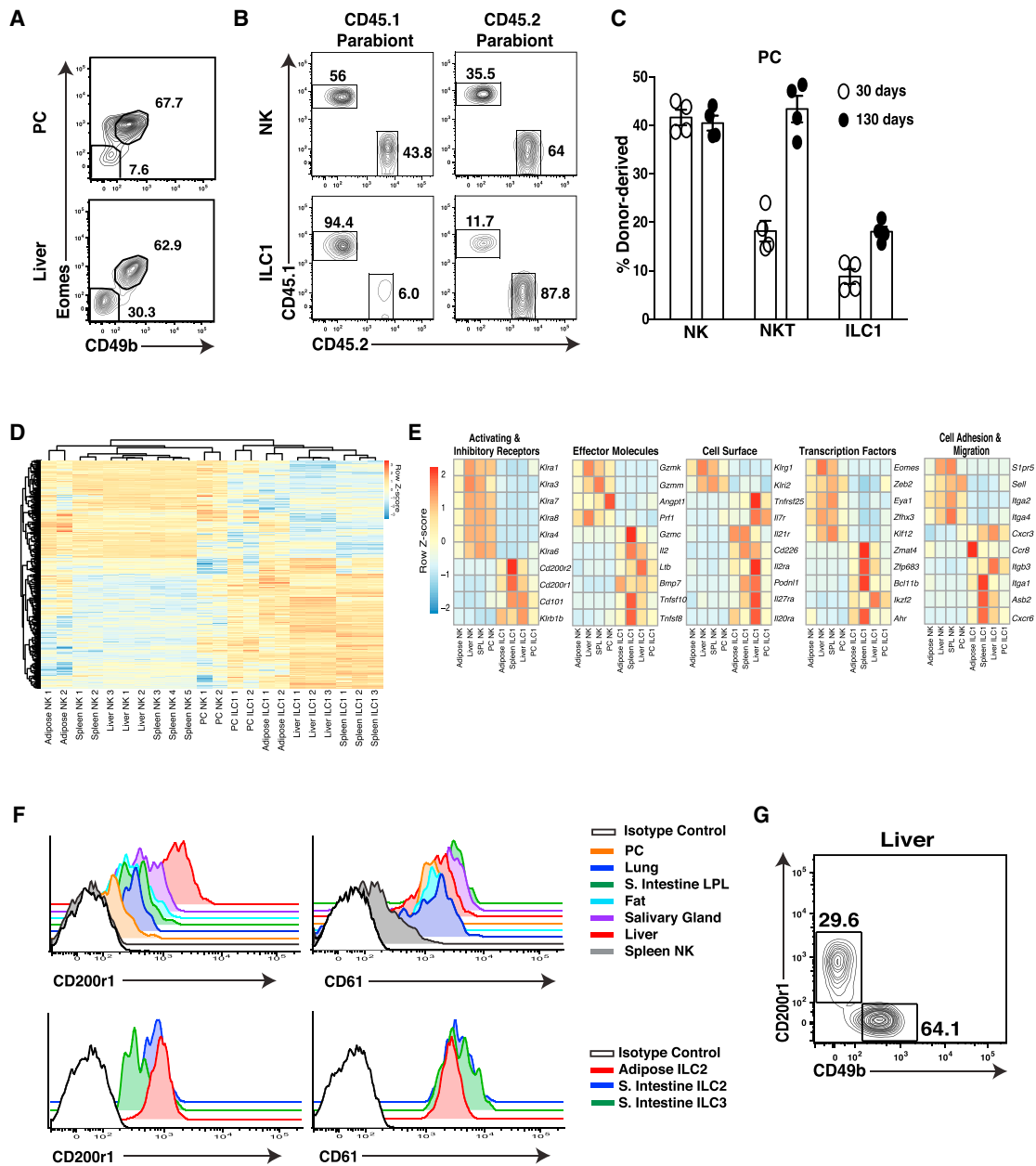


Figure 2. PC and Liver-Resident ILC1 Are Distinct from Circulating NK Cells

(A) Representative plots are gated on total group 1 ILCs (Lin⁻NKp46⁺NK1.1⁺Tbet⁺) and show Eomes and CD49b expression in the PC and liver of WT mice (Lin⁻CD3ε⁺TCRβ⁺CD19⁺F4/80⁺).

(B and C) Parabiotic mice were generated by surgically connecting CD45.1⁺ and CD45.2⁺ mice for 30 and 130 days. (B) Representative plots show host and donor-derived NK cells (CD49b⁺Eomes⁺) and ILC1 (CD49b⁻Eomes⁻) and (C) percentage of donor-derived populations in the PC (NKT = CD45⁺CD19⁻F4/80⁻TCRβ⁺CD3ε⁺NK1.1⁺).

(D and E) RNA-sequencing (RNA-seq) reveals gene expression signature of the indicated cell populations sort purified from *Eomes*-GFP mice. (D) Differential gene expression across all samples for all genes with FDR-adjusted p value less than 10⁻⁵ (713 total). (E) Gene expression signature of all samples indicated by a manually curated representative subset from (D). Heatmap shows data pooled from biological replicates (see the STAR Methods).

(F) Histograms show CD200r1 and CD61 expression on resting splenic NK cells and ILC1 from indicated tissues (top), and on resting NK cells, ILC1, ILC2, and ILC3 from the small intestine lamina propria of WT mice (bottom).

(G) Representative plot shows CD200r1 and CD49b expression on Lin⁻NKp46⁺NK1.1⁺Tbet⁺ cells in the liver of WT mice. Data are representative of 2–3 independent experiments with (A, F, G) n = 5 mice, (B and C), n = 3–4 parabiotic pairs, and (D and E) n = 40–50 mice per group.

See also Figures S1 and S2 and Tables S1 and S2.

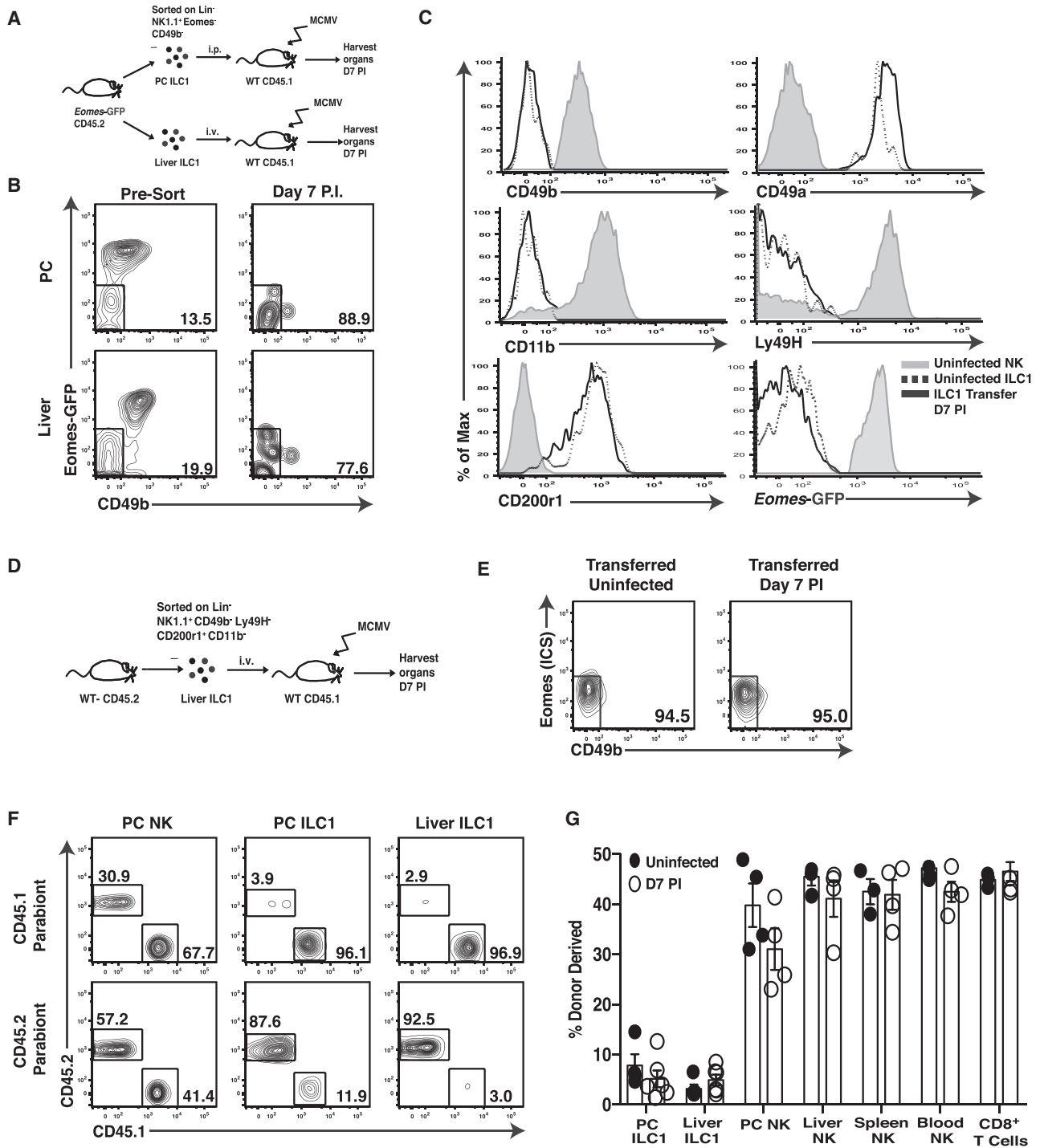


Figure 3. ILC1s Represent a Stable Lineage during Viral Infection

(A) Schematic of experiment. Briefly, 1×10^4 PC ILC1 and 3.5×10^5 liver ILC1 ($CD45.2^+Lin^-NK1.1^+Eomes^+CD49b^-$) were sorted from *Eomes-GFP* mice and adoptively transferred into separate $CD45.1^+$ WT mice, i.p. or intravenously (i.v.), respectively. Mice were subsequently infected with MCMV and analyzed at 7 days PI.

(B) Plots show ILC1 from the PC and livers of uninfected *Eomes-GFP* mice (left plots) and following transfer and MCMV infection (day 7 PI, right plots).

(C) Histograms show indicated cell surface markers on liver ILC1 and NK cells from uninfected *Eomes-GFP* mice, and adoptively transferred liver ILC1 at 7 days PI.

(D) Schematic of experiment. 4×10^4 liver ILC1 ($Lin^-NK1.1^+CD49a^+CD49b^-CD200r1^+CD11b^-Ly49h^-$) were sorted from $CD45.2^+$ mice, adoptively transferred i.v. into $CD45.1^+$ WT mice, and subsequently infected with MCMV.

(legend continued on next page)

contained transcription factors, cell-adhesion molecules, cell surface receptors, and effector molecules (Figures 2E and S2B). The transcription factor *Zfp683* (a *Blimp1* homolog also known as Hobit), which has been implicated in controlling T_{RM} and liver ILC1 tissue-residency and survival (Mackay et al., 2016), was highly enriched in all ILC1 and not expressed by NK cells (Figure 2E). In contrast, whereas all ILC1 shared enriched transcripts for *Il7r*, *Itga1* (CD49a), and *Cxcr6* compared to low expression by NK cells, these and other markers associated with tissue-resident lymphocytes, such as CD69 and CD103, were not homogeneously expressed on all peripheral ILC1 (Figures 2E and S2D), making them unsuitable as lineage-defining markers. In contrast, we found that ILC1 were enriched for transcripts of the inhibitory receptor CD200r1 and the cell surface integrin CD61 (*tgb3*) (Figure 2E), which were expressed on the cell surface of all peripheral ILC1 analyzed, and on ILC2 and ILC3 in the small intestine and adipose tissue (Figures 2F and 2G), albeit at different levels. Because we observed little to no expression of CD61 and CD200r1 on peripheral NK cells (Figure S3; data not shown), our results suggest that these markers will be more useful than previously described markers to discriminate NK cells from all other ILCs.

Tissue-Resident ILC1 Are Distinct from Circulating NK Cells during MCMV-Induced Inflammation

During homeostasis, parabiotic mouse and lineage-tracing experiments have been used to show that liver and adipose NK cells and ILC1 are stable phenotypic and functional lineages (Daussy et al., 2014; O'Sullivan et al., 2016; Peng et al., 2013; Sojka et al., 2014). However, whether differences between NK cells and ILC1 are lost during viral-induced inflammation is unknown. To test whether ILC1 could differentiate into NK cells (and vice versa), we sorted CD49b⁻Eomes⁻ PC and liver ILC1 and control splenic CD49b⁺Eomes⁺ NK cells to high purity from *Eomes*-GFP mice, adoptively transferred them into congenically distinct WT hosts, and infected with MCMV (Figure 3A and S3A). A week later, we observed that CD49b⁻Eomes⁻ ILC1 from both tissues maintained a stable phenotype (Figure 3B) and remained CD49b⁻CD11b⁻CD49a⁺Eomes⁻CD200r1⁺ in recipient mice (Figure 3C). Furthermore, ILC1 did not acquire the NK cell-specific activating receptor Ly49H (Figure 3C), suggesting that ILC1 are not an immature form of NK cells at homeostasis that differentiate following acute inflammation, but rather a distinct and stable lineage. Adoptively transferred splenic CD49b⁺Eomes⁺ NK cells increased expression of markers associated with an ILC1 phenotype, such as CD69 as early as 36 hr PI (Figure S3B) and CD49a and CD61 1 week following infection (Figure S3C). However, NK cells did not express CD200r1 (Figures S3B and S3C) and did not lose expression of NK cell lineage-defining molecules such as Eomes, Ly49H, or CD49b at these time points following infection (Figure S3C). These results suggest that although NK cells can increase CD49a, CD69, and

CD61 expression in a cell-autonomous fashion following viral infection, they do not phenotypically convert to ILC1.

To further confirm that endogenous ILC1 are a stable lineage during inflammation, we sorted purified CD200r1⁺Ly49H⁻CD49b⁻CD11b⁻ liver ILC1 and adoptively transferred these cells into congenically distinct hosts and infected with MCMV (Figure 3D). One week later, liver ILC1 remained CD49b⁻Eomes⁻ by intracellular staining (Figure 3E). An important functional characteristic of ILCs is their maintenance of tissue-residency during acute inflammation (Gasteiger et al., 2015). Indeed, PC and liver ILC1 remained strongly tissue-resident at homeostasis and following MCMV infection of parabiotic mice (Figures 3F and 3G). In contrast, NK cells were derived from the circulation in peripheral tissues (Figures 3F and 3G), suggesting that even activated NK cells do not become tissue-resident following MCMV infection. Collectively, these results strongly suggest that the PC and the liver contain phenotypically and functionally distinct lineages of ILC1 and NK cells during viral-induced inflammation.

ILC1 Are the Main Early Source of IFN- γ at Initial Sites of Infection

Because total group 1 ILCs and IFN- γ were required to restrain viral replication in primary infected tissues (Figure 1), and Ly49H-dependent NK cell responses are responsible for systemic host protection to MCMV in C57BL/6 mice (Brown et al., 2001), we analyzed whether NK cells or ILC1 produced more IFN- γ early following viral infection in barrier and non-barrier tissues. Notably, we found that only ILC1 in the PC, liver, and lung produced robust amounts of IFN- γ in vivo early after infection with several viruses, including MCMV (i.p., h.d., and i.n.), SeV (i.n.) and PR8 influenza virus (i.n.), compared to all other known IFN- γ -producing lymphocytes (Figures 4A–4C and S4A–S4E; data not shown). This early IFN- γ response was restricted to the primary site of infection, before the initiation of any other IFN- γ response in other peripheral organs (Figures 4A–4C). ILC1 produced more IFN- γ compared to NK cells in the PC, liver, and lung following tissue-specific infection (Figures 4C–4F; data not shown), suggesting that tissue-resident ILC1 are the first and main producers of IFN- γ in virally infected tissues prior to the initiation of circulating NK cell responses.

Liver ILC1 Are Required for Limiting Early Viral Replication and Enhancing Host Survival

To test whether ILC1 responses were required for restricting viral replication and promoting host tissue protection following MCMV infection, we utilized *Zfp683*^{-/-} (Hobit-deficient) mice that are severely reduced in liver ILC1 (Mackay et al., 2016), but not circulating NK cells or other peripheral ILC1 (Figures 5A and S5A–S5C), and *Nkp46*^{Cre/+} x *Eomes*^{fl/fl} (called NK-*Eomes*^{-/-} hereafter) mice that selectively lack circulating NK cells (Gordon et al., 2012), but not tissue-resident ILC1 (Figures 5A and S5B). Hydrodynamic infection of these mice resulted in

(E) Representative plots show CD49b and intracellular Eomes staining of adoptively transferred ILC1 recovered in the liver at 7 days PI. (F and G) Parabiotic mice were generated and both parabionts infected with MCMV i.p. Organs were analyzed at day 7 PI for chimerism of indicated lymphocyte populations. (F) Representative plots and (G) percentage of donor-derived NK cells and ILC1 shown for indicated organs. Data are representative of 3 independent experiments with (A–E) n = 3–4 mice and (F and G) n = 3–4 parabiotic pairs per group. See also Figure S3.

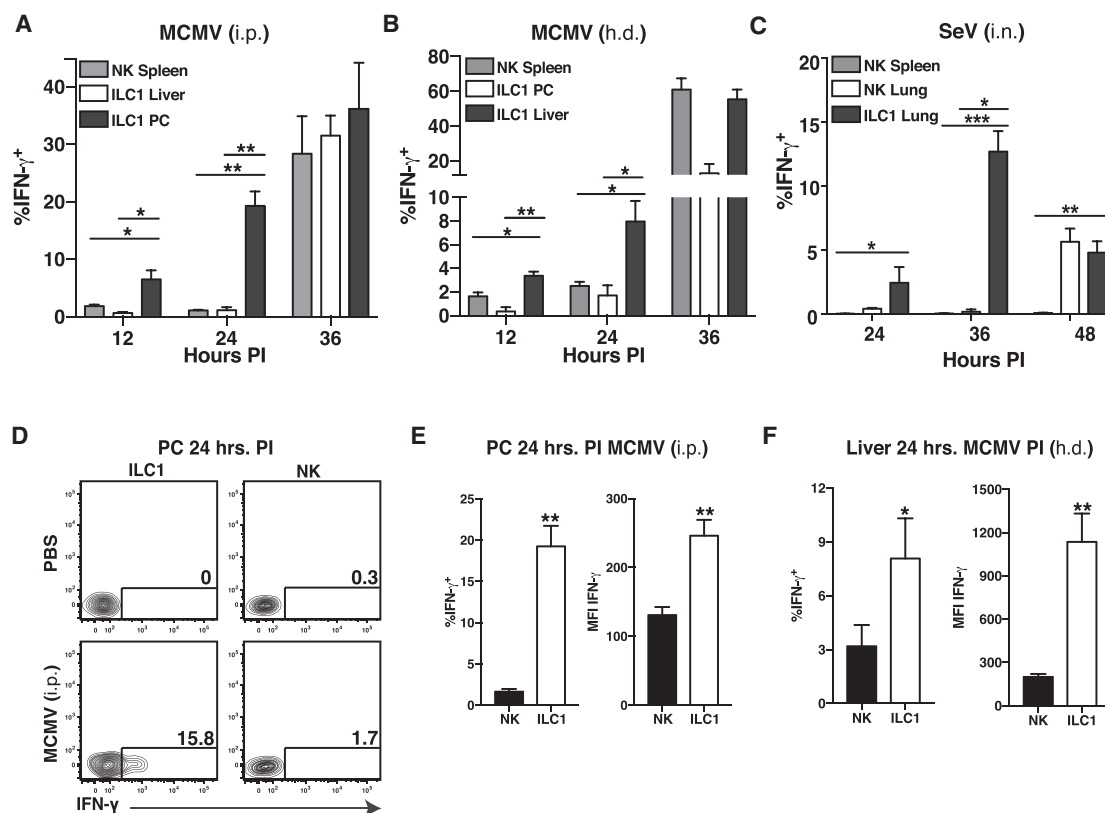


Figure 4. ILC1 Rapidly Produce IFN- γ Early during Host Anti-viral Responses at Initial Sites of Infection in Naive Hosts

WT mice were infected with MCMV either i.p. or h.d. or SeV i.n., and peripheral tissues were harvested and analyzed for intracellular IFN- γ staining.

(A and B) Quantification of intracellular IFN- γ staining of indicated group 1 ILC populations at various time points following either MCMV (i.p.) (A) or MCMV (h.d.) (B).

(C) Quantification of intracellular IFN- γ staining of indicated group 1 ILC populations at various time points following SeV (i.n.) infection in i.v. unlabeled fraction of indicated organ.

(D) Flow plots show intracellular IFN- γ staining of NK cells and ILC1 in PC at 24 hr PI (MCMV, i.p.).

(E and F) Quantification of intracellular IFN- γ staining by percentage and MFI of NK cells and ILC1 in (E) PC (MCMV, i.p.) or (F) liver (MCMV, h.d.) at 24 hr PI. Data are representative of 3–4 independent experiments with $n = 5$ –7 mice per group. Samples were compared using an unpaired, two-tailed Student's t test, and data are presented as the mean \pm SEM (* $p < 0.05$, ** $p < 0.01$, *** $p < 0.001$).

See also Figure S4.

increased viral loads in the liver of Hobit-deficient mice similar to total group 1 ILC-deficient (α -NK1.1-treated) mice (Figure 5B). In contrast, NK-*Eomes*^{-/-} mice showed low viral burden similar to WT controls (Figure 5B), suggesting that Hobit-dependent liver ILC1, but not *Eomes*-dependent NK cells, are required for early control of MCMV infection. Higher viral loads in Hobit-deficient mice were likely due to lack of liver ILC1, as we observed similar recruitment (Figure S5D) and IFN- γ production from Hobit-deficient liver NK cells (Figures S5E and S5F) in *Zfp683*^{-/-}:WT mixed bone marrow chimeric mice. Next, we tested whether liver ILC1 were critical for limiting systemic viral dissemination to contribute to host survival. Hydrodynamic infection of Hobit-deficient mice resulted in increased MCMV titers in the blood and led to rapid lethality similar to total group 1 ILC-depleted mice and distinct from WT controls that survived the infection (Figures 5C and 5D). These results suggest that Hobit-dependent ILC1 rapidly restrict virus replication and dissemination to ensure host survival.

To determine whether liver ILC1-derived IFN- γ was sufficient to limit early viral replication in the absence of other lymphocytes, we transferred WT or *Irfng*^{-/-} liver ILC1 into *Rag2*^{-/-} \times *Il2rg*^{-/-} mice and challenged with MCMV (Figure 5E). Adoptively transferred WT ILC1, but not *Irfng*^{-/-} ILC1, were able to suppress virus in recipients similar to ILC1-sufficient *Rag2*^{-/-} mice (Figure 5F), suggesting that liver ILC1-derived IFN- γ is sufficient to control early MCMV replication at the initial site of infection. PC ILC1 are also likely required for host antiviral protection in the absence of *Nfil3*-dependent NK cells, because depletion of total NK1.1⁺ cells in *Nfil3*^{-/-} mice (Figure S6A) lead to higher viral titers in the PC and greater viral dissemination (Figure S6B).

Tissue-Resident cDC1 Produce Local IL-12 Early after Infection to Drive Optimal IFN- γ Production by ILC1

IFN- γ responses are preceded by local proinflammatory cytokine responses mediated by myeloid lineage cells at sites of

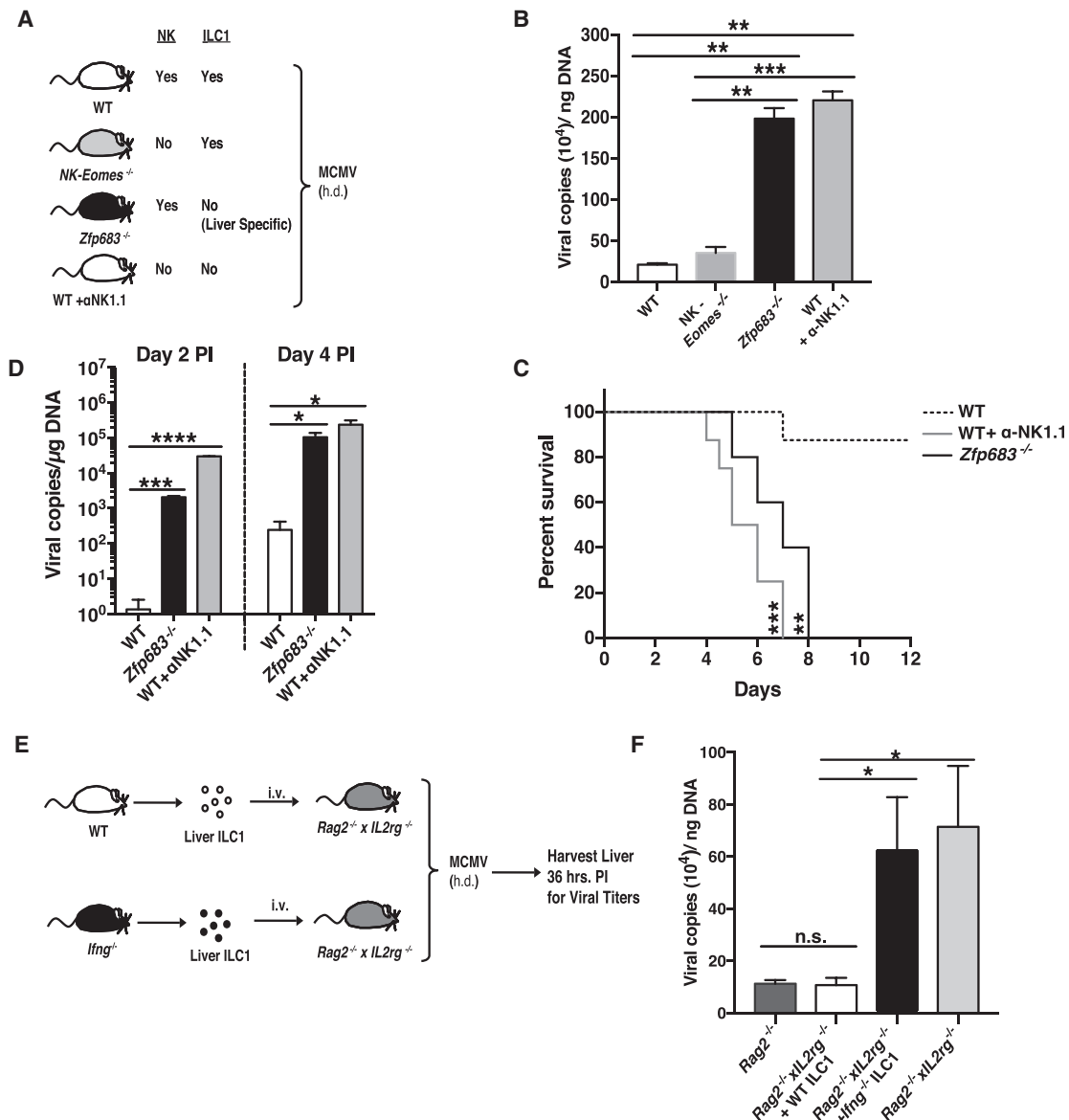


Figure 5. Production of IFN- γ by ILC1 Confers Early Host Anti-viral Protection at Initial Sites of Infection

(A–D) (A) Schematic of experiment. WT, NK-Eomes^{-/-}, Zfp683^{-/-} (Hobit-deficient), and WT mice treated with α -NK1.1 were infected with MCMV by h.d. injection. Viral titers of each indicated cohort are shown for (B) the liver at 36 hr PI and (C) the peripheral blood at day 2 and 4 PI. (D) Kaplan-Meier survival curves of each indicated cohort.

(E) Schematic of experiment. 4×10^4 liver ILC1 from either WT or *Ifng*^{-/-} mice were adoptively transferred i.v. into separate Rag2^{-/-} x IL2rg^{-/-} recipients and subsequently infected with MCMV by h.d. injection.

(F) Viral titers of each indicated cohort are shown for liver at 36 hr PI. Data are representative of 3–4 independent experiments with $n = 5$ –7 mice per group. Samples were compared using an unpaired, two-tailed Student's *t* test, and data are presented as the mean \pm SEM (* $p < 0.05$, ** $p < 0.01$, *** $p < 0.001$, **** $p < 0.0001$).

See also Figures S5 and S6.

infection through TLR-dependent mechanisms during MCMV infection (Biron and Tarrio, 2015). Early host protective cytokine production consists of discrete waves of IFN- α , IFN- β , and the proinflammatory IL-12 and IL-18, among other cytokines (Biron and Tarrio, 2015). Therefore, we investigated which proinflammatory cytokine signals are required for tissue-resident ILC1

production of IFN- γ during infection. Both liver NK cells and ILC1 did not require type I interferon signaling for optimal IFN- γ production; however, these populations had an absolute requirement for IL-12 signaling, as *Il12rb2*^{-/-} or *Stat4*^{-/-} NK cells and ILC1 showed more than 95% reduction in IFN- γ production compared to WT controls (Figure 6A). Furthermore,

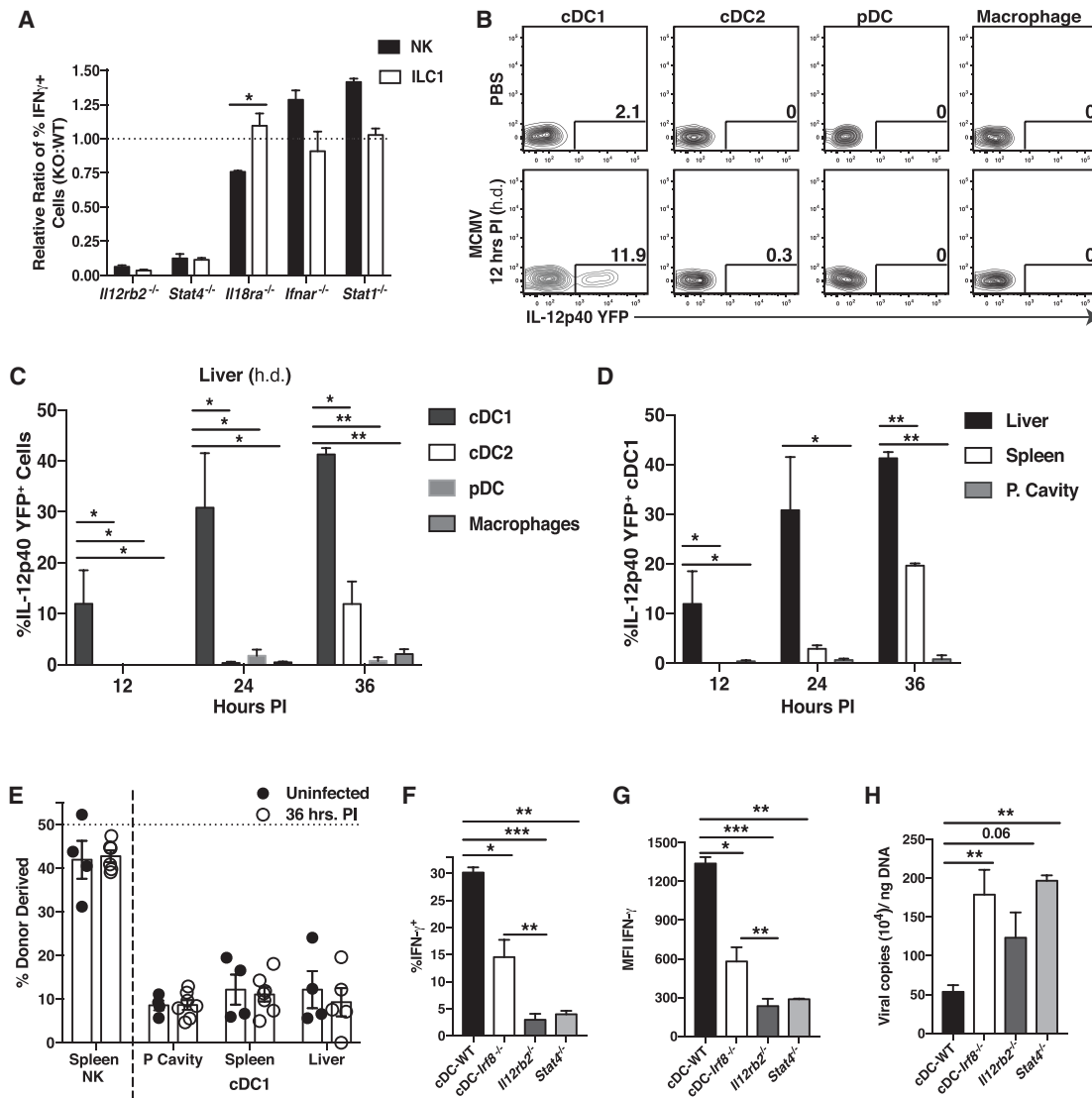


Figure 6. Tissue-Resident cDC1 Rapidly Produce IL-12 during Viral Infection to drive Optimal IFN- γ Production by ILC1

(A) Mixed bone marrow chimeras (mBMC) harboring WT (CD45.1⁺) and selected proinflammatory cytokine receptors- or STAT molecule-deficient (CD45.2⁺) bone marrow were infected at 8 weeks following reconstitution with MCMV (i.p. injection). Intracellular IFN- γ production was assessed at 36 hr PI in the PC, and data are represented as the relative ratio of IFN- γ production of KO to WT cells within each infected chimeric mouse.

(B–D) *Il-12p40*-YFP reporter mice were infected with MCMV by h.d. injection and peripheral tissues were harvested and analyzed for YFP⁺ cells at various time points PI (cDC1 = CD45⁺Lin⁻CD64⁻MHCII^{hi}CD11c^{hi}CD11b⁻XCR1⁺, cDC2 = CD45⁺Lin⁻CD64⁻MHCII^{hi}CD11c^{hi}XCR1⁻CD11b⁺, pDC = CD45⁺Lin⁻CD64⁻MHCII⁺CD11c⁺CD11b⁻XCR1⁻B220⁺, macrophage = CD45⁺Lin⁻CD64⁺MHCII⁺CD11b⁺). (B) Flow plots and (C) graphs show percentages of YFP⁺ cells in different liver populations at 12, 24, and 36 hr PI. (D) Quantification of YFP⁺ cDC1 in peripheral tissues at 12, 24, and 36 hr PI.

(E) Parabiotic mice were generated and both parabionts were infected with MCMV i.p. Percentage of donor-derived spleen NK cells and cDC1 in indicated organs at 36 hr PI.

(F–H) WT, cDC-*Irf8*^{-/-}, *Il12rb2*^{-/-}, and *Stat4*^{-/-} mice were infected with MCMV by h.d. injection and analyzed at 36 hr PI. Graphs show (F) percentage and (G) MFI of IFN- γ -expressing liver ILC1, and (H) viral titers in the liver within each group. Data are representative of 2 independent experiments with (A–E) n = 3–4 and (F and G) n = 5–7 mice per group. Samples were compared using an unpaired, two-tailed Student's t test, and data are presented as the mean \pm SEM (*p < 0.05, **p < 0.01, ***p < 0.001).

See also Figure S7.

ILC1 were distinct from NK cells in that they did not require IL-18 signaling for optimal production of IFN- γ (Figure 6A).

Because macrophages, conventional dendritic cells (cDC), and plasmacytoid dendritic cells (pDC) have all been described

to produce IL-12 in vivo during pathogen challenge (Alexandre et al., 2014; Trinchieri, 2003), we utilized *Il-12p40*-YFP reporter mice to determine the major cellular source of local IL-12 in virally infected tissues. Unbiased analysis of total YFP⁺ cells revealed

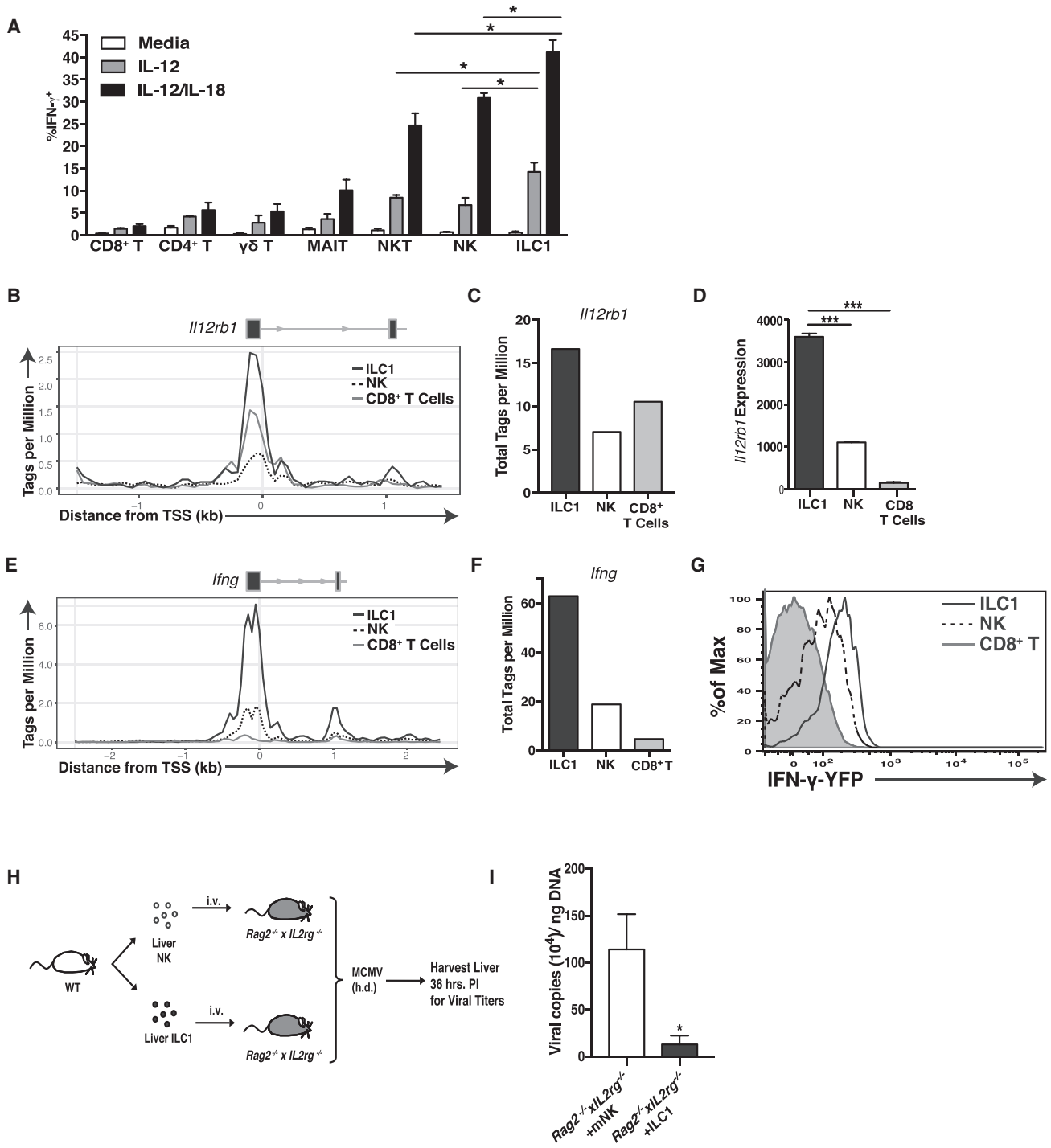


Figure 7. ILC1 Are the Most Responsive to IL-12 among IFN- γ Producing Lymphocytes

(A) Graph shows percentage of IFN- γ ⁺ cells within indicated liver populations following stimulation with either media alone, IL-12, or IL-12 plus IL-18 (CD8⁺ T = TCR β ⁺CD3⁺CD8 α ⁺ MR-1⁻, CD4⁺ T = TCR β ⁺CD3⁺CD4⁺ MR-1⁻, γ δ T = CD3⁺TCR γ / δ ⁺, MAIT = CD3⁺MR-1⁺).

(B and C) ATAC-sequencing (ATAC-seq) peaks (B) and (C) quantification of peaks (C), mapping to *Il12rb1* promoter (1.5 kb upstream and downstream of the transcriptional start site) in resting ILC1, NK cells, and CD8⁺ T cells. *Il12rb1* exons are shown as black boxes with black arrows denoting the origin and directionality of transcription.

(D) RNA-seq reads mapping to *Il12rb1* in the indicated populations.

(E and F) ATAC-seq peaks (E) and quantification of peaks (F), mapping to *Ifng* promoter (2.5 kb upstream and downstream of the transcriptional start site) in resting ILC1, NK cells, and CD8⁺ T cells.

(legend continued on next page)

that the majority of IL-12 producing cells at 12 hr PI in the PC and liver, or at 36 hr PI in the lung, respectively, were CD64⁺CD11c^{hi}MHCII^{hi}CD11b⁻XCR1⁺ cells (Figure S7A; data not shown). This phenotype is consistent with a “cDC1” population that has been shown to be important in viral cross-presentation and induction of oral tolerance in the gut (Durai and Murphy, 2016; Esterházy et al., 2016). Furthermore, we did not observe YFP⁺ macrophages, pDCs, or CD11b⁺XCR1⁻ cDC2s (Figures 6B, 6C, and S7B–S7E; data not shown), suggesting that cDC1s are the major early producers of IL-12 in virally infected tissues. This early IL-12 response was restricted to initial sites of infection and preceded known systemic production of IL-12 at 36 hr PI following MCMV infection (Figures 6D and S7D). IL-12 is likely produced by cDC1 in a local and tissue-resident manner, as this subset of dendritic cells remained strongly host-derived in parabiotic mice following viral infection (Figure 6E and S7F).

Previous studies have shown that the cDC lineage can be marked by expression of the transcription factor *Zbtb46*, and cDC1 require IRF8 in a cell-intrinsic manner for their development (Durai and Murphy, 2016; Esterházy et al., 2016; Satpathy et al., 2012). Therefore, we used *Zbtb46*^{Cre/+} × *Irf8*^{fl/fl} mice (called cDC-*Irf8*^{-/-} hereafter) to specifically ablate this subset in vivo (Figures S7G and S7H). Systemic deletion of the cDC1 lineage lead to decreased IFN- γ production in liver ILC1 compared to littermate controls (*Zbtb46*^{+/+} × *Irf8*^{fl/fl} called cDC-WT) (Figures 6F and 6G). Although the observed reduction of liver ILC1-produced IFN- γ in cDC-*Irf8*^{-/-} mice was not as pronounced in *Il12rb2*^{-/-} or *Stat4*^{-/-} mice (Figures 6F and 6G), we observed similar increases in viral titers (Figure 6H), suggesting that the diminished IFN- γ secretion by ILC1 in cDC-*Irf8*^{-/-} mice was not sufficient to efficiently limit early viral replication. Thus, these results suggest that local IL-12 produced by tissue-resident cDC1 contributes to optimal IFN- γ production by ILC1 to confer early host protection at infected tissue sites.

ILC1 Are Poised for Greatest IFN- γ Production in Response to Proinflammatory Cytokines

Although NK cells and other unconventional adaptive lymphocytes can produce IFN- γ in an antigen independent-manner during MCMV infection (Ninomiya et al., 2000; Sun et al., 2012; Wesley et al., 2008), the responsiveness, kinetics, and effector function of all of these cells relative to each other are unknown. During ex vivo stimulation with IL-12, or IL-12 and IL-18, we observed that ILC1 produced the most IFN- γ , with fewer NK, NKT, and other adaptive lymphocytes cells producing IFN- γ that was more dependent on IL-18 (Figure 7A). These results suggest that liver ILC1 as a population are the most responsive to proinflammatory cytokines in their ability to produce IFN- γ .

In support of this hypothesis, we performed transposase-accessible chromatin (ATAC) sequencing and analyzed the *Il12rb1* promoter in resting ILC1, NK, and CD8⁺ T cells. We found

that ILC1 showed greatest chromatin accessibility at the *Il12rb1* promoter (Figures 7B and 7C) and highest amount of *Il12rb1* transcripts as measured by RNA sequencing (Figure 7D), in support of ILC1 possessing a heightened ability to sense IL-12 in their environment. Additionally, ILC1 showed greatest *Irfng* promoter accessibility (Figures 7E and 7F) and highest *Irfng* transcripts in IFN- γ -YFP mice (Figure 7G). Altogether, these results suggest that ILC1 may be epigenetically or transcriptionally poised to produce more IFN- γ than NK or CD8⁺ T cells. Consistent with these findings, we found that adoptive transfer of liver ILC1 into *Rag2*^{-/-} × *Il2rg*^{-/-} mice can limit early viral replication to a greater extent than an equal number of NK cells (Figures 7H and 7I; data not shown). Together, these results place tissue-resident ILC1 on the top of a functional spectrum of rapid IFN- γ -producing lymphocytes during local infection.

DISCUSSION

ILCs have been proposed to be the “first responders” of the lymphocyte lineage based on their tissue-residency and ability to rapidly respond to local environmental signals in an antigen-independent manner (Artis and Spits, 2015; Serafini et al., 2015). Here, we demonstrate a critical early role for ILC1, but not other innate or adaptive lymphocytes, in limiting viral replication via rapid production of IFN- γ at the initial site of infection. NK cells and unconventional T cell subsets did not produce IFN- γ until afterward, suggesting that these previously considered “early” antiviral lymphocyte responses occur later than tissue-resident ILC1 responses. Although our study has focused on early tissue-resident lymphocyte responses in naive mice, virus-specific effector T cells can give rise to tissue-resident memory T cells (T_{RM}) following primary infection that rapidly and robustly control secondary pathogen challenge in an antigen-dependent manner by inducing potent host antiviral immunity (Ariotti et al., 2014; Schenkel et al., 2014). However, using a model of heterologous secondary infection, we observed that early lung ILC1 IFN- γ responses still preceded influenza-primed CD8⁺ T_{RM} responses following challenge with Sendai virus four weeks later (O.-E.W., J.C.S., and T.E.O. unpublished observations), suggesting that ILC1 responses may still confer early host viral protection even in the presence of bystander CD8⁺ T_{RM} responses.

During MCMV infection, some virus will eventually disseminate from primary infected tissues, and thus additional innate and adaptive lymphocytes such as NK cells, CD8⁺ T cells, CD4⁺ T cells, and $\gamma\delta$ T cells have been shown to participate in limiting viral replication at later stages of infection and in secondary organ sites (Klenerman and Oxenius, 2016; Lanier, 2008; Ninomiya et al., 2000). Among these responses, NK cells are critical in limiting viral replication within the first week and precede the contribution of antigen-specific T and B cell responses that are

(G) Histogram shows percentage of YFP⁺ cells within liver NK cells, ILC1, and CD8⁺ T cells from *Irfng*-YFP reporter (GREAT) mice.

(H) Schematic of experiment. 3×10^4 liver ILC1 and 6×10^4 liver NK cells were adoptively transferred into *Rag2*^{-/-} × *Il2rg*^{-/-} recipients and at 7 days post-transfer (when equal numbers of ILC1 and NK cell can be recovered in the liver), recipient mice were challenged with MCMV by h.d. injection.

(I) Graph shows the viral titers within the liver of each group at 36 hr PI. ATAC-seq data represent 1 experiment of 15 pooled mice per population, and the rest of the data are representative of 2–3 experiments of 4–6 mice per group. Samples were compared using an unpaired, two-tailed Student's t test, and data are presented as the mean \pm SEM (*p < 0.05, ***p < 0.001).

critical at later times post-infection (Brown et al., 2001; Kleverman and Oxenius, 2016; Lanier, 2008). Similarly, our results highlight the complementary but essential functions of both innate and adaptive lymphocytes to combat MCMV, which has co-evolved with the mammalian host to evade immune surveillance at multiple stages. These results indicate that although certain ILC responses may be inconsequential in the presence of adaptive immunity (Rankin et al., 2015; Vély et al., 2016), there are conditions when ILC1 are critical for optimal host control of viral infection. Therefore, we propose a model in which tissue-resident cDCs and ILC1 serve the earliest role in local MCMV control during an early phase (0–36 hr), which is followed by a critical intermediate phase consisting of circulating anti-viral NK cell responses (36 hr–7 days) and finally a late phase consisting of antigen-specific T and B cell responses (7–30 days) to cooperatively limit systemic viral burden. This essential and diverse response of tissue-resident and circulating type 1 lymphocytes may represent an evolutionary adaptation required for specialization of a layered immune response during specific pathogen encounters.

In agreement with our proposed role for ILC1 in host defense, recent studies have suggested that intestinal ILC1 represent the major IFN- γ producing innate lymphocyte population in response to pathogenic microbes and are required for host protection during infection of mice with *Toxoplasma gondii*, *Salmonella enterica*, or following acute oral infection of the opportunistic pathogen *Clostridium difficile* (Abt et al., 2015; Klose et al., 2013, 2014). However, these studies used T-bet-deficient mice, which have reduced numbers of mature ILC1 and mature NK cells (Deng et al., 2015; O'Sullivan et al., 2016; Townsend et al., 2004), to conclude that intestinal ILC1 are required for host microbial protection. T-bet has also been shown to be required for NK cell IFN- γ production and migration and the development of NKp46⁺ ILC3s (Jenne et al., 2009; Rankin et al., 2013; Townsend et al., 2004). Therefore, the results from these studies were not able to definitively distinguish between the contribution of IFN- γ production by NK cells, ILC1, and ILC3 to the reported protective phenotypes. Using Hobit-deficient mice, we believe our results now provide a more precise assessment of the contribution of tissue-resident ILC1 to host immunity, as these mice lack liver ILC1 but not other ILCs (Mackay et al., 2016). Although a recent study reported that Hobit-deficient mice display reduced frequencies of liver NKT cells that are functionally defective in granzyme B production following MCMV infection (van Gisbergen et al., 2012), we did not observe lower numbers of liver NKT cells in Hobit-deficient mice. Furthermore, because NKT cells are not required for early control of MCMV in the liver or spleen (van Dommelen et al., 2003), the defects in survival and control of virus observed in Hobit-deficient mice are unlikely attributable to this population. In addition, we found that Hobit was not required for NK cell production of IFN- γ or cDC1 production of IL-12 following MCMV infection. Hobit is not required for the generation of effector T cells (Mackay et al., 2016) and is not expressed at appreciable levels in other myeloid-lineage cells (Immunological Genome Project), suggesting that the diminished early antiviral protection we observed in the liver of Hobit-deficient mice was due to loss of liver ILC1. Although future work will further elucidate the role of ILC1 in intestinal

antimicrobial defense (using models of specific ILC1 deletion or ILC1-specific ablation of IFN- γ), our study clearly delineates a role for ILC1 in limiting viral replication at sites of initial infection.

Unbiased whole-genome epigenetic and transcriptomic signatures collectively suggested that mature mouse and human ILCs contain distinct regulomes (i.e., epigenetic landscapes controlled by chromatin modifications that regulate gene expression) that allow for their functional and phenotypic distinction during homeostasis on a population and single cell level (Gury-BenAri et al., 2016; Koues et al., 2016; Shih et al., 2016). Recently, studies have suggested that NK cells represent only one member of a heterogeneous group of type 1 innate lymphoid cells (Artis and Spits, 2015; Serafini et al., 2015). However, a key challenge is selecting definitive criteria to discriminate NK cells from other group 1 ILCs at steady state and during immune responses. Eomes, CD49a, CD49b, and TRAIL are differentially expressed by each group 1 ILC within different peripheral organs during homeostasis (Cortez et al., 2014; Daussy et al., 2014; Gordon et al., 2012; Klose et al., 2014; O'Sullivan et al., 2016; Sojka et al., 2014), but it is unclear whether these characteristics can be modulated by the activation state of the cells during inflammation, injury, or infection. From our RNA sequencing analysis, we identified the markers CD61 and CD200r1 as highly expressed on peripheral tissue-resident ILCs, but either barely or not expressed by circulating NK cells. Furthermore, the combined expression of CD200r1, Eomes, and CD49b can differentiate ILC1 from NK cells during homeostasis and viral-induced inflammation. It should be noted that specific markers previously associated with the ILC1 lineage, such as CD49a and CD69, can be expressed by activated NK cells and are not uniformly expressed by all peripheral ILC1. These results provide strong evidence that these previous markers should not be used to identify ILC1, whereas CD61 and CD200r1 will be more useful in future studies.

Given the diversity and rapid effector function of tissue-resident lymphocytes (Fan and Rudensky, 2016), there is a growing need to more precisely understand the biology of tissue-resident cells in health and disease. Here, we present an ILC1 signature distinct from circulating NK cells and show that ILC1 maintain lineage stability during viral-induced inflammation. Our findings reveal that tissue-resident ILC1 function to limit early viral replication at primary sites of infection through rapid production of IFN- γ in response to local production of IL-12 by cDC1. Thus, ILC1 contribute to host immunity as tissue-resident “sentinels” in viral immunosurveillance at sites of primary viral entry.

STAR★METHODS

Detailed methods are provided in the online version of this paper and include the following:

- KEY RESOURCES TABLE
- CONTACT FOR REAGENT AND RESOURCE SHARING
- EXPERIMENTAL MODEL AND SUBJECT DETAILS
 - Mice
 - Viruses
- METHOD DETAILS
 - Mouse Techniques
 - In vivo Virus Infection

- Virus quantification
- Isolation of lymphocytes
- Flow cytometry and cell sorting
- Adoptive transfer experiments
- Ex vivo stimulation of lymphocytes
- RNA sequencing
- ATAC Sequencing
- **QUANTIFICATION AND STATISTICAL ANALYSIS**
 - RNA Sequencing Analysis
 - ATAC analysis
 - Statistical analyses
- **DATA AVAILABILITY**

SUPPLEMENTAL INFORMATION

Supplemental Information includes seven figures and two tables and can be found with this article online at <https://doi.org/10.1016/j.cell.2017.09.052>.

AUTHOR CONTRIBUTIONS

O.-E.W., J.C.S., M.A.D.-E., and T.E.O. designed the study. O.-E.W., N.M.A., I.S., and T.E.O. performed the experiments. C.L., Y.P., C.K., and C.S.L. performed RNA-seq and ATAC-seq bioinformatics analysis. T.E.O., O.-E.W., and J.C.S. wrote the manuscript.

ACKNOWLEDGMENTS

We thank members of the Sun lab for helpful comments and discussions. We thank E. Pamer, V. Lazarevic, K.P. van Gisbergen, M. Li, and D. Mucida for mice. We thank L. Lanier, B. Moltedo, X. Fan, and A. Chaudhry for helpful discussions. T.E.O. was supported by the American Cancer Society. N.M.A. was supported by the NIH Medical Scientist Training Program grant T32GM07739 to the Weill Cornell/Rockefeller/Sloan Kettering Tri-Institutional MD-PhD Program. M.A.D.-E. and I.S. were supported by an NHMRC Fellowship (1119298 to M.A.D.-E.) and NHMRC grants (1125357, 1071822). J.C.S. was supported by the Ludwig Center for Cancer Immunotherapy, the Burroughs Wellcome Fund, the American Cancer Society, and grants from the NIH (AI100874, AI130043, and P30CA008748).

Received: May 17, 2017

Revised: August 11, 2017

Accepted: August 16, 2017

Published: October 19, 2017

REFERENCES

- Abt, M.C., Lewis, B.B., Caballero, S., Xiong, H., Carter, R.A., Sušac, B., Ling, L., Leiner, I., and Pamer, E.G. (2015). Innate immune defenses mediated by two ILC subsets are critical for protection against acute *Clostridium difficile* infection. *Cell Host Microbe* *18*, 27–37.
- Alexandre, Y.O., Cocita, C.D., Ghilas, S., and Dalod, M. (2014). Deciphering the role of DC subsets in MCMV infection to better understand immune protection against viral infections. *Front. Microbiol.* *5*, 378.
- Ariotti, S., Hogenbirk, M.A., Dijkgraaf, F.E., Visser, L.L., Hoekstra, M.E., Song, J.Y., Jacobs, H., Haanen, J.B., and Schumacher, T.N. (2014). T cell memory. Skin-resident memory CD8⁺ T cells trigger a state of tissue-wide pathogen alert. *Science* *346*, 101–105.
- Artis, D., and Spits, H. (2015). The biology of innate lymphoid cells. *Nature* *517*, 293–301.
- Biron, C.A., and Tarrío, M.L. (2015). Immunoregulatory cytokine networks: 60 years of learning from murine cytomegalovirus. *Med. Microbiol. Immunol. (Berl.)* *204*, 345–354.
- Brown, M.G., Dokun, A.O., Heusel, J.W., Smith, H.R., Beckman, D.L., Blattenberger, E.A., Dubbelde, C.E., Stone, L.R., Scalzo, A.A., and Yokoyama, W.M. (2001). Vital involvement of a natural killer cell activation receptor in resistance to viral infection. *Science* *292*, 934–937.
- Buenrostro, J.D., Giresi, P.G., Zaba, L.C., Chang, H.Y., and Greenleaf, W.J. (2013). Transposition of native chromatin for fast and sensitive epigenomic profiling of open chromatin, DNA-binding proteins and nucleosome position. *Nat. Methods* *10*, 1213–1218.
- Cortez, V.S., Fuchs, A., Cella, M., Gilfillan, S., and Colonna, M. (2014). Cutting edge: salivary gland NK cells develop independently of Nfil3 in steady-state. *J. Immunol.* *192*, 4487–4491.
- Daussy, C., Faure, F., Mayol, K., Viel, S., Gasteiger, G., Charrier, E., Biennu, J., Henry, T., Debien, E., Hasan, U.A., et al. (2014). T-bet and Eomes instruct the development of two distinct natural killer cell lineages in the liver and in the bone marrow. *J. Exp. Med.* *211*, 563–577.
- Deng, Y., Kerdiles, Y., Chu, J., Yuan, S., Wang, Y., Chen, X., Mao, H., Zhang, L., Zhang, J., Hughes, T., et al. (2015). Transcription factor Foxo1 is a negative regulator of natural killer cell maturation and function. *Immunity* *42*, 457–470.
- Durai, V., and Murphy, K.M. (2016). Functions of murine dendritic cells. *Immunity* *45*, 719–736.
- Esterházy, D., Loschko, J., London, M., Jove, V., Oliveira, T.Y., and Mucida, D. (2016). Classical dendritic cells are required for dietary antigen-mediated induction of peripheral T(reg) cells and tolerance. *Nat. Immunol.* *17*, 545–555.
- Fan, X., and Rudensky, A.Y. (2016). Hallmarks of tissue-resident lymphocytes. *Cell* *164*, 1198–1211.
- Franklin, R.A., Liao, W., Sarkar, A., Kim, M.V., Bivona, M.R., Liu, K., Pamer, E.G., and Li, M.O. (2014). The cellular and molecular origin of tumor-associated macrophages. *Science* *344*, 921–925.
- Gasteiger, G., Fan, X., Dikiy, S., Lee, S.Y., and Rudensky, A.Y. (2015). Tissue residency of innate lymphoid cells in lymphoid and nonlymphoid organs. *Science* *350*, 981–985.
- Geiger, T.L., Abt, M.C., Gasteiger, G., Firth, M.A., O'Connor, M.H., Geary, C.D., O'Sullivan, T.E., van den Brink, M.R., Pamer, E.G., Hanash, A.M., and Sun, J.C. (2014). Nfil3 is crucial for development of innate lymphoid cells and host protection against intestinal pathogens. *J. Exp. Med.* *211*, 1723–1731.
- Godfrey, D.I., Uldrich, A.P., McCluskey, J., Rossjohn, J., and Moody, D.B. (2015). The burgeoning family of unconventional T cells. *Nat. Immunol.* *16*, 1114–1123.
- Goldrath, A.W., and Bevan, M.J. (1999). Selecting and maintaining a diverse T-cell repertoire. *Nature* *402*, 255–262.
- Gordon, S.M., Chaix, J., Rupp, L.J., Wu, J., Madera, S., Sun, J.C., Lindsten, T., and Reiner, S.L. (2012). The transcription factors T-bet and Eomes control key checkpoints of natural killer cell maturation. *Immunity* *36*, 55–67.
- Gury-BenAri, M., Thaïss, C.A., Serafini, N., Winter, D.R., Giladi, A., Lara-Astiaso, D., Levy, M., Salame, T.M., Weiner, A., David, E., et al. (2016). The spectrum and regulatory landscape of intestinal innate lymphoid cells are shaped by the microbiome. *Cell* *166*, 1231–1246.
- Hermesh, T., Moltedo, B., Moran, T.M., and López, C.B. (2010). Antiviral instruction of bone marrow leukocytes during respiratory viral infections. *Cell Host Microbe* *7*, 343–353.
- Iwasaki, A., and Medzhitov, R. (2004). Toll-like receptor control of the adaptive immune responses. *Nat. Immunol.* *5*, 987–995.
- Iwasaki, A., and Medzhitov, R. (2015). Control of adaptive immunity by the innate immune system. *Nat. Immunol.* *16*, 343–353.
- Jenkins, M.K., Chu, H.H., McLachlan, J.B., and Moon, J.J. (2010). On the composition of the preimmune repertoire of T cells specific for Peptide-major histocompatibility complex ligands. *Annu. Rev. Immunol.* *28*, 275–294.
- Jenne, C.N., Enders, A., Rivera, R., Watson, S.R., Bankovich, A.J., Pereira, J.P., Xu, Y., Roots, C.M., Beilke, J.N., Banerjee, A., et al. (2009). T-bet-dependent S1P5 expression in NK cells promotes egress from lymph nodes and bone marrow. *J. Exp. Med.* *206*, 2469–2481.

- Kamimura, Y., and Lanier, L.L. (2014). Rapid and sequential quantitation of salivary gland-associated mouse cytomegalovirus in oral lavage. *J. Virol. Methods* **205**, 53–56.
- Kim, D., Langmead, B., and Salzberg, S.L. (2015). HISAT: a fast spliced aligner with low memory requirements. *Nat. Methods* **12**, 357–360.
- Klenerman, P., and Oxenius, A. (2016). T cell responses to cytomegalovirus. *Nat. Rev. Immunol.* **16**, 367–377.
- Klose, C.S., Kiss, E.A., Schwierzeck, V., Ebert, K., Hoyler, T., d'Hargues, Y., Göppert, N., Croxford, A.L., Waisman, A., Tanriver, Y., and Diefenbach, A. (2013). A T-bet gradient controls the fate and function of CCR6-ROR γ t+ innate lymphoid cells. *Nature* **494**, 261–265.
- Klose, C.S.N., Flach, M., Möhle, L., Rogell, L., Hoyler, T., Ebert, K., Fabianke, C., Pfeifer, D., Sexl, V., Fonseca-Pereira, D., et al. (2014). Differentiation of type 1 ILCs from a common progenitor to all helper-like innate lymphoid cell lineages. *Cell* **157**, 340–356.
- Koues, O.I., Collins, P.L., Cella, M., Robinette, M.L., Porter, S.I., Pyfrom, S.C., Payton, J.E., Colonna, M., and Oltz, E.M. (2016). Distinct gene regulatory pathways for human innate versus adaptive lymphoid cells. *Cell* **165**, 1134–1146.
- Lanier, L.L. (2008). Evolutionary struggles between NK cells and viruses. *Nat. Rev. Immunol.* **8**, 259–268.
- Liao, Y., Smyth, G.K., and Shi, W. (2013). The Subread aligner: fast, accurate and scalable read mapping by seed-and-vote. *Nucleic Acids Res.* **41**, e108.
- Liu, F., Song, Y., and Liu, D. (1999). Hydrodynamics-based transfection in animals by systemic administration of plasmid DNA. *Gene Ther.* **6**, 1258–1266.
- Loh, J., Chu, D.T., O'Guin, A.K., Yokoyama, W.M., and Virgin, H.W., 4th. (2005). Natural killer cells utilize both perforin and gamma interferon to regulate murine cytomegalovirus infection in the spleen and liver. *J. Virol.* **79**, 661–667.
- Love, M.I., Huber, W., and Anders, S. (2014). Moderated estimation of fold change and dispersion for RNA-seq data with DESeq2. *Genome Biol.* **15**, 550.
- Mackay, L.K., Minnich, M., Kragten, N.A., Liao, Y., Nota, B., Seillet, C., Zaid, A., Man, K., Preston, S., Freestone, D., et al. (2016). Hobit and Blimp1 instruct a universal transcriptional program of tissue residency in lymphocytes. *Science* **352**, 459–463.
- Mudge, J.M., and Harrow, J. (2015). Creating reference gene annotation for the mouse C57BL6/J genome assembly. *Mamm. Genome* **26**, 366–378.
- Nguyen, K.B., Salazar-Mather, T.P., Dalod, M.Y., Van Deusen, J.B., Wei, X.Q., Liew, F.Y., Caligiuri, M.A., Durbin, J.E., and Biron, C.A. (2002). Coordinated and distinct roles for IFN- α beta, IL-12, and IL-15 regulation of NK cell responses to viral infection. *J. Immunol.* **169**, 4279–4287.
- Ninomiya, T., Takimoto, H., Matsuzaki, G., Hamano, S., Yoshida, H., Yoshikai, Y., Kimura, G., and Nomoto, K. (2000). V γ 1+ γ delta T cells play protective roles at an early phase of murine cytomegalovirus infection through production of interferon- γ . *Immunology* **99**, 187–194.
- O'Sullivan, T.E., Sun, J.C., and Lanier, L.L. (2015). Natural killer cell memory. *Immunity* **43**, 634–645.
- O'Sullivan, T.E., Rapp, M., Fan, X., Weizman, O.E., Bhardwaj, P., Adams, N.M., Walzer, T., Dannenberg, A.J., and Sun, J.C. (2016). Adipose-resident group 1 innate lymphoid cells promote obesity-associated insulin resistance. *Immunity* **45**, 428–441.
- Paya, C.V., Hermans, P.E., Wiesner, R.H., Ludwig, J., Smith, T.F., Rakela, J., and Krom, R.A. (1989). Cytomegalovirus hepatitis in liver transplantation: prospective analysis of 93 consecutive orthotopic liver transplantations. *J. Infect. Dis.* **160**, 752–758.
- Peng, H., Jiang, X., Chen, Y., Sojka, D.K., Wei, H., Gao, X., Sun, R., Yokoyama, W.M., and Tian, Z. (2013). Liver-resident NK cells confer adaptive immunity in skin-contact inflammation. *J. Clin. Invest.* **123**, 1444–1456.
- Rankin, L.C., Groom, J.R., Chopin, M., Herold, M.J., Walker, J.A., Mielke, L.A., McKenzie, A.N., Carotta, S., Nutt, S.L., and Belz, G.T. (2013). The transcription factor T-bet is essential for the development of NKp46+ innate lymphocytes via the Notch pathway. *Nat. Immunol.* **14**, 389–395.
- Rankin, L., Girard-Madoux, M., Seillet, C., Mielke, L., Kerdiles, Y., Fenis, A., Wieduwild, E., Putoczki, T., Mondot, S., Lantz, O., et al. (2015). Complementarity and redundancy of IL-22-producing innate lymphoid cells. *Nat. Immunol.* **17**, 179–186.
- Robinette, M.L., Fuchs, A., Cortez, V.S., Lee, J.S., Wang, Y., Durum, S.K., Gilfillan, S., and Colonna, M.; Immunological Genome Consortium (2015). Transcriptional programs define molecular characteristics of innate lymphoid cell classes and subsets. *Nat. Immunol.* **16**, 306–317.
- Salazar-Mather, T.P., Orange, J.S., and Biron, C.A. (1998). Early murine cytomegalovirus (MCMV) infection induces liver natural killer (NK) cell inflammation and protection through macrophage inflammatory protein 1 α (MIP-1 α)-dependent pathways. *J. Exp. Med.* **187**, 1–14.
- Satpathy, A.T., Kc, W., Albring, J.C., Edelson, B.T., Kretzer, N.M., Bhattacharya, D., Murphy, T.L., and Murphy, K.M. (2012). Zbtb46 expression distinguishes classical dendritic cells and their committed progenitors from other immune lineages. *J. Exp. Med.* **209**, 1135–1152.
- Schenkel, J.M., and Masopust, D. (2014). Tissue-resident memory T cells. *Immunity* **41**, 886–897.
- Schenkel, J.M., Fraser, K.A., Beura, L.K., Pauken, K.E., Vezys, V., and Masopust, D. (2014). T cell memory. Resident memory CD8 T cells trigger protective innate and adaptive immune responses. *Science* **346**, 98–101.
- Serafini, N., Vosshenrich, C.A., and Di Santo, J.P. (2015). Transcriptional regulation of innate lymphoid cell fate. *Nat. Rev. Immunol.* **15**, 415–428.
- Shih, H.Y., Sciumè, G., Mikami, Y., Guo, L., Sun, H.W., Brooks, S.R., Urban, J.F., Jr., Davis, F.P., Kanno, Y., and O'Shea, J.J. (2016). Developmental acquisition of regulomes underlies innate lymphoid cell functionality. *Cell* **165**, 1120–1133.
- Sojka, D.K., Plougastel-Douglas, B., Yang, L., Pak-Wittel, M.A., Artyomov, M.N., Ivanova, Y., Zhong, C., Chase, J.M., Rothman, P.B., Yu, J., et al. (2014). Tissue-resident natural killer (NK) cells are cell lineages distinct from thymic and conventional splenic NK cells. *eLife* **3**, e01659.
- Sun, J.C., Beilke, J.N., and Lanier, L.L. (2009). Adaptive immune features of natural killer cells. *Nature* **457**, 557–561.
- Sun, J.C., Madera, S., Bezman, N.A., Beilke, J.N., Kaplan, M.H., and Lanier, L.L. (2012). Proinflammatory cytokine signaling required for the generation of natural killer cell memory. *J. Exp. Med.* **209**, 947–954.
- Townsend, M.J., Weinmann, A.S., Matsuda, J.L., Salomon, R., Farnham, P.J., Biron, C.A., Gapin, L., and Glimcher, L.H. (2004). T-bet regulates the terminal maturation and homeostasis of NK and Valpha14i NKT cells. *Immunity* **20**, 477–494.
- Trinchieri, G. (2003). Interleukin-12 and the regulation of innate resistance and adaptive immunity. *Nat. Rev. Immunol.* **3**, 133–146.
- van Dommelen, S.L., Tabarias, H.A., Smyth, M.J., and Degli-Esposti, M.A. (2003). Activation of natural killer (NK) T cells during murine cytomegalovirus infection enhances the antiviral response mediated by NK cells. *J. Virol.* **77**, 1877–1884.
- van Gisbergen, K.P., Kragten, N.A., Hertoghs, K.M., Wensveen, F.M., Jonjic, S., Hamann, J., Nolte, M.A., and van Lier, R.A. (2012). Mouse Hobit is a homolog of the transcriptional repressor Blimp-1 that regulates NKT cell effector differentiation. *Nat. Immunol.* **13**, 864–871.
- Vély, F., Barlogis, V., Vallentin, B., Neven, B., Piperoglou, C., Ebbo, M., Perchet, T., Petit, M., Yessaad, N., Touzot, F., et al. (2016). Evidence of innate lymphoid cell redundancy in humans. *Nat. Immunol.* **17**, 1291–1299.
- von Andrian, U.H., and Mackay, C.R. (2000). T-cell function and migration. Two sides of the same coin. *N. Engl. J. Med.* **343**, 1020–1034.
- Wesley, J.D., Tessmer, M.S., Chaukos, D., and Brossay, L. (2008). NK cell-like behavior of Valpha14i NK T cells during MCMV infection. *PLoS Pathog.* **4**, e1000106.

STAR★METHODS

KEY RESOURCES TABLE

REAGENT or RESOURCE	SOURCE	IDENTIFIER
Antibodies		
Anti-Mouse NK1.1	Tonbo Biosciences	PK136
Anti-Mouse CD3e	Tonbo Biosciences	17A2
Anti-Mouse Ly6G	Tonbo Biosciences	1A8
Anti-Mouse B220	Tonbo Biosciences	RA3-6B2
Anti-Mouse IFN- γ	Tonbo Biosciences	XMG1.2
Anti-Mouse CD11b	BioLegend	M1/70
Anti-Mouse CD19	BioLegend	ID3
Anti-Mouse CD49b/DX5	BioLegend	DX5
Anti-Mouse KLRG1	BioLegend	2F1
Anti-Mouse NKp46	BioLegend	29A1.4
Anti-Mouse CD45.1	BioLegend	A20
Anti-Mouse CD45	BioLegend	30-F11
Anti-Mouse CD45.2	BioLegend	104
Anti-Mouse CD8 α	BioLegend	53-6.7
Anti-Mouse CD4	BioLegend	GK1.5
Anti-Mouse TCR β	BioLegend	H57-597
Anti-Mouse TCR $\gamma\delta$	BioLegend	GL3
Anti-Mouse CD90.2	BioLegend	30-H12
Anti-Mouse Tbet	BioLegend	4B10
Anti-Mouse CD200r1	BioLegend	OX-110
Anti-Mouse CD61	BioLegend	2C9.G2
Anti-Mouse CD69	BioLegend	H1.2F3
Anti-Mouse CD103	BioLegend	2E7
Anti-Mouse F4/80	BioLegend	BM8.1
Anti-Mouse CD11c	BioLegend	N418
Anti-Mouse XCR1	BioLegend	ZET
Anti-Mouse MHCII	BioLegend	M5.114.14.2
Anti-Mouse CD64	BioLegend	X54-57.1
PE Rat IgG2a, k Isotype Control	BioLegend	RTK2758
PE Armenian Hamster IgG Isotype Control	BioLegend	HTK888
Anti-Mouse Eomes	eBioscience	Dan11mag
Anti-Mouse Ly49H	eBioscience	3D10
Anti-Mouse CD49a	BD	Ha31/8
Anti-Mouse CD16/CD32	BD	2.4G2
MR-1 Tetramer	NIH	N/A
NK1.1 ⁺ depletion antibody	JC. Sun (PI)	PK136
IFN- γ blocking antibody	BioLegend	H22
Ly49H blocking antibody	W. Yokoyama (PI)	3D10
Bacterial and Virus Strains		
Murine Cytomegalovirus	JC. Sun (PI)	Smith Strain
Sendai Virus	ATCC	Cantell Strain (VR-907)
Influenza A	A. Rudensky (PI)	PR8 Strain

(Continued on next page)

Continued

REAGENT or RESOURCE	SOURCE	IDENTIFIER
Chemicals, Peptides, and Recombinant Proteins		
Brefeldin A	Sigma	Cat# B7651
Monensin (GolgiStop)	BD Biosciences	Cat# 554724
Recombinant Mouse IL-12	R&D Systems	Cat# 419-ML
Recombinant Mouse IL-18	MBL	Cat# B002-5
Critical Commercial Assays		
RNeasy Mini Kit	QIAGEN	Cat# 74106
DNA Mini Kit	QIAGEN	Cat# 51304
Trizol	Thermo Fischer Scientific	Cat# 15596026
Cytofix/Cytoperm	BD Biosciences	Cat# 554714
Foxp3/Transcription Factor Staining Buffer	Thermo Fisher Scientific	Cat# 00-5523-00
SuperScript III Reverse Transcriptase	Thermo Fischer Scientific	Cat# 18080044
iQ SYBR Green Supermix	Biorad	Cat# 1708880
Deposited Data		
Raw Data Files for RNA Sequencing	NCBI Gene Expression Omnibus	RNA Sequencing Database: GSE 103901
Raw Data Files for ATAC Sequencing	NCBI Gene Expression Omnibus	ATAC Sequencing Database: GSE 103900
Experimental Models: Organisms/Strain		
Mouse: C57BL/6 (CD45.2)	Jackson Lab	Stock # 000664
<i>Irfng</i> -YFP (GREAT mice).	Jackson Lab	Stock # 017581
<i>Il12p40</i> -YFP	Jackson Lab	Stock # 006412
Mouse: B6.SJL (CD45.1)	Jackson Lab	Stock # 002114
Mouse: <i>Rag2</i> ^{-/-}	Jackson Lab	Stock # 008449
Mouse: <i>Rag2</i> ^{-/-} <i>xIl2rg</i> ^{-/-}	Jackson Lab	Stock # 014593
Mouse: <i>Eomes</i> ^{GFP} transgenic	T. Walzer (PI) (Daussy et al., 2014)	N/A
Mouse: <i>Il12rb2</i> ^{-/-} , <i>Stat4</i> ^{-/-} , <i>Il18ra1</i> ^{-/-} , <i>Stat1</i> ^{-/-} , <i>Ifnar</i> ^{-/-} , <i>Klra8</i> ^{-/-} (Ly49H-deficient), <i>Nfil3</i> ^{-/-}	JC. Sun (PI)	N/A
Mouse: <i>Zbtb46</i> ^{Cre} <i>x Irf8</i> ^{fl/fl}	D. Mucida (PI)	N/A
Mouse: <i>Nkp46</i> ^{Cre} <i>x Eomes</i> ^{fl/fl}	V. Lazarevic (PI)	N/A
Mouse: <i>Zfp683</i> ^{-/-}	K.P. van Gisbergen (PI) & M. LI	N/A
Mouse: <i>Tbx21</i> ^{-/-} , <i>Irfng</i> ^{-/-}	E. Pamer (PI)	N/A
Oligonucleotides		
Primers against MCMV IE-1 (F: TCGCCATCGTTTCGAGA, R: TCTCGTAGGTCCACTGACCGA)	(Kamimura and Lanier, 2014)	N/A
Primers against SeV P (F: CCAAGAGAGCGTGAATCAT R: GGGTCAAACCTGGTAGCCTT)	(Hermesh et al., 2010)	N/A
Primers against mouse β -actin (F: AGGTGACAGCATTGC TTCTG R: GCTGCCTCAACACCTCAAC)	(Hermesh et al., 2010)	N/A
Software and Algorithms		
FastQC	Simon Andrews	https://www.bioinformatics.babraham.ac.uk/projects/fastqc/
HISAT2 v2.05	(Kim et al., 2015)	https://ccb.jhu.edu/software/hisat2/index.shtml
Rsubread	(Liao et al., 2013)	https://bioconductor.org/packages/release/bioc/html/Rsubread.html
DESeq2	(Love et al., 2014)	https://bioconductor.org/packages/release/bioc/html/DESeq2.html
pheatmap R package	Raivo Kolde	https://cran.r-project.org/web/packages/pheatmap/index.html
bwa v0.7.12	Li H. and Durbin R	http://bio-bwa.sourceforge.net

CONTACT FOR REAGENT AND RESOURCE SHARING

Further information and requests for resources and reagents should be directed to and will be fulfilled by the Lead Contact, Timothy O'Sullivan (tosullivan@mednet.ucla.edu)

EXPERIMENTAL MODEL AND SUBJECT DETAILS

Mice

Mice were bred at Memorial Sloan Kettering Cancer Center in accordance with the guidelines of the institutional Animal Care and Use Committee (IACUC). The following mouse strains were used in this study: C57BL/6 (CD45.2), B6.SJL (CD45.1), *Rag2*^{-/-}, *Rag2*^{-/-}*xIl2rg*^{-/-}, *Eomes*^{GFP} transgenic (Daussy et al., 2014), *Tbx21*^{-/-}, *Nkp46*^{Cre} x *Eomes*^{fl/fl}, *Nfil3*^{-/-}, *Klra8*^{-/-} (Ly49H-deficient), *Zfp683*^{-/-}, *Ifng*^{-/-}, *Il12rb2*^{-/-}, *Stat4*^{-/-}, *Il18ra1*^{-/-}, *Ifnar*^{-/-}, *Stat1*^{-/-}, *Il12p40*-YFP, *Zbtb46*^{Cre} x *Irf8*^{fl/fl}, and *Ifng*-YFP (GREAT mice). Experiments were conducted using age- and gender-matched mice in accordance with approved institutional protocols.

Viruses

MCMV (Smith or K181 strain) was serially passaged through BALB/c hosts three times, and then salivary gland viral stocks were prepared with a dounce homogenizer for dissociating the salivary glands of infected mice 3 weeks after infection. Sendai virus (Cantell strain) and Influenza virus (PR8 Strain) were grown in 10 day embryonated chicken eggs (SPAFAS; Charles River Laboratories). Eggs allantoic fluid was snap frozen in ethanol-dry ice bath and stored at -80°C.

METHOD DETAILS

Mouse Techniques

Generation of mixed bone marrow chimeric mice was performed as previously described (Sun et al., 2009). Parabiosis surgery was performed as previously described (Franklin et al., 2014; Gasteiger et al., 2015). Briefly, 6-8 week old female congenic CD45.2 and CD45.1 mice were surgically connected in parabiosis. After lateral skin incisions were made from the elbow to knee in each mouse, forelimbs and hind limbs were tied together using nylon suture, and the skin incisions were closed using stainless steel wound clips. After surgery, mice were maintained on a diet supplemented with trimethoprim/sulfamethoxazole for prophylaxis against infection. Intravascular labeling of lymphocytes of experimental mice was performed by injecting (i.v.) 2.5 µg of fluorophore-conjugated CD45 (30-F11) and euthanized 3 min later.

In vivo Virus Infection

Experimental mice in studies were infected with MCMV by i.p. injection of 7.5×10^3 plaque-forming units (PFU) in 0.5 mL or by hydrodynamic injection (h.d.) of 4×10^4 PFU in 2.0 mL or 1×10^6 PFU in 0.05 mL by intranasal injection (i.n.) of MCMV. For survival experimental studies, mice were injected with 5×10^3 PFU in 2.0 mL by h.d. injection. Hydrodynamic injection was performed as previously described (Liu et al., 1999) to deliver virus directly to the liver. Experimental mice in studies were infected with SeV (Cantell Strain) by i.n. injection of 1×10^4 PFU or with Influenza (PR8-Strain) by i.n. injection of 5×10^2 PFU in 0.04 mL. In some experiments mice were injected twice i.p. with either 200 µg of α -NK1.1 (PK136), 200 µg of α -IFN- γ (H22), or 200 µg of α -Ly49H (3D10) 3 days and 1 day before infection.

Virus quantification

MCMV viral titers were determined as previously described (Kamimura and Lanier, 2014). DNA was isolated from peripheral blood, PC, or Liver; using a genomic purification kit (QIAGEN). Following isolation, DNA concentration was measured using Nanodrop for each sample, and 3 µL was added into mastermix containing iQ Sybr Green (Bio-Rad) and primers specific to MCMV IE-1 DNA (F: TCGCCATCGTTTCGAGA, R: TCTCGTAGGTCCACTGACCGA). Copy number was determined by comparing Cq values to a standard curve of known dilutions of an MCMV plasmid and normalized relative to total DNA content. Liver and PC viral titers were normalized to weight of organ and volume of peritoneal gavage respectively.

SeV viral particles were determined by qRT-PCR as previously described (Hermesh et al., 2010). Lungs were harvested after infection and homogenized in 2 mL TRIzol reagent (Thermo Fisher). RNA was isolated from TRIzol according to the manufacturer's protocol. cDNA was synthesized using SuperScript Reverse Transcriptase (Thermo Fisher) and quantitative PCR was performed using SYBR-Green (Bio-Rad) on a CFX Connect instrument (Bio-Rad). SeV RNA was detected using primers designed to SEV P (F: CCAAGAGAGCGTGGAATCAT R: GGGTCAAACCTGGTAGCCTT). SeV P RNA levels were normalized to β -actin (F: AGGTGA CAGCATTGCTTCTG R: GCTGCCTCAACACCTCAAC) using the 2- $\Delta\Delta$ CT method.

Isolation of lymphocytes

Spleens were dissociated using glass slides and filtered through a 100-µm strainer. To isolate lamina propria lymphocytes (LPL), small intestines were removed and flushed, and Peyer's patches were excised. The intestines were then opened up lengthwise and sliced transversely into 0.5 cm-long pieces, which were incubated in 1 mM dithiothreitol and 1 mM EDTA for 15 min to remove

intraepithelial lymphocytes (IEL). After IEL were removed, the pieces of intestine were incubated in digest solution (1 mg/mL collagenase and 1 U/mL DNase I in RPMI supplemented with 5% fetal calf serum, 1% L-glutamine, 1% penicillin-streptomycin, and 10 mM HEPES) for 30 min, passed through a 100- μ m strainer, and purified using 40% Percoll. To isolate lymphocytes from liver, the tissues were physically dissociated using a glass tissue homogenizer and purified using a discontinuous gradient of 40% over 60% Percoll. To isolate the stromal vascular fraction (SVF) of adipose tissue, visceral adipose tissue was physically dissociated using scissors and incubated for 40 min in digest solution (2mg/ml type II collagenase in RPMI supplemented with 5% fetal calf serum, 1% L-glutamine, 1% penicillin-streptomycin, and 10 mM HEPES). Resulting dissociated tissue was passed through 100- μ m strainers, centrifuged, and adipocytes were removed from the supernatant. To isolate cells from the peritoneal cavity, 4 mL of PBS with 3% fetal calf serum was injected into the peritoneal cavity and wash (containing cells) extracted using a 27 g needle and filtered through a 40- μ m strainer. To isolate cells from the lung and the salivary gland, the tissue was physically dissociated using scissors and incubated for 30 min in digest solution (1mg/ml type D collagenase in RPMI supplemented with 5% fetal calf serum, 1% L-glutamine, 1% penicillin-streptomycin, and 10 mM HEPES). Resulting dissociated tissue was passed through 100- μ m strainers, centrifuged, and lymphocytes were removed from the supernatant. Salivary gland lymphocytes were further purified using 40% Percoll. Red blood cells in spleen, adipose, liver, lung, salivary gland, and PC were lysed using ACK lysis buffer.

Flow cytometry and cell sorting

Cell surface staining of single-cell suspensions from various organs was performed using fluorophore-conjugated antibodies (BD Biosciences, eBioscience, BioLegend, Tonbo, R&D Systems) Flow cytometry antibodies used in analysis of purified lymphocytes can be found below. Intracellular staining was performed by fixing and permeabilizing with the eBioscience Foxp3/Transcription Factor Staining Set for staining intranuclear proteins. Intracellular staining for IFN- γ was performed using the Cytofix/Cytoperm kit (BD Biosciences) after 4 hr incubation of single cell suspension of lymphocytes in RPMI containing 10% fetal bovine serum with Brefeldin A (10 μ g/mL, Sigma).

Flow cytometry and cell sorting were performed on the LSR II and Aria II cytometers (BD Biosciences), respectively. Data were analyzed with FlowJo software (Tree Star). *I12p40*-YFP fluorescence was quantified in peripheral tissues by normalizing to steady state fluorescence of YFP⁺ cells in uninfected control mice. Cell surface staining was performed using the following fluorophore-conjugated antibodies - NK1.1 (PK136), CD11b (M1/70), CD19 (ID3), CD49b/DX5 (DX5), KLRG1 (2F1), NKp46 (29A1.4), CD45.1 (A20), CD45 (30-F11), CD45.2 (104), CD8 α (53-6.7), CD4 (GK1.5), TCR β (H57-597), Eomes (Dan11mag), CD3e (17A2), TCR $\gamma\delta$ (GL3), Ly6G (1A8), CD90.2 (30- H12), T-bet (4B10), Ly49H (3D10), CD200r1 (OX-110), CD49a (Ha31/8), CD61(2C9.G2), CD69(H1.2F3), CD103(2E7) F4/80 (BM8.1), CD11c (N418), IFN- γ (XMG1.2), MR-1 (NIH Tetramer Core), MHCII (M5/114.14.2), B220 (RA3-6B2), CD64 (X54-5/7.1), XCR1 (ZET).

Adoptive transfer experiments

NK cells and ILC1 were purified from liver, PC, or spleen from either CD45.2⁺ *Eomes*-GFP or CD45.2⁺ WT mice, by flow cytometric cell sorting to high purity and transferred into CD45.1⁺ WT or Ly49H-deficient recipients and were infected with MCMV 1 day post adoptive transfer. In other experiments, NK cells and ILC1 were purified from liver of WT or *Irfng*^{-/-} by flow cytometric cell sorting to high purity and transferred into *Rag2*^{-/-}*Il2rg*^{-/-} recipients and infected with MCMV 7 days following adoptive transfer.

Ex vivo stimulation of lymphocytes

Approximately 3×10^5 liver lymphocytes were stimulated for 5 hr in RPMI containing 10% fetal bovine serum with recombinant mouse IL-12 (20 ng/ml; R&D Systems) plus IL-18 (10 ng/ml; R&D Systems). Cells were cultured in media alone as a negative control.

RNA sequencing

For RNA sequencing, RNA was isolated from sorted cell populations from *Eomes*-GFP using TRIzol (Invitrogen) followed by SMARTer amplification and Illumina next-generation sequencing.

ATAC Sequencing

For ATAC sequencing, ATAC-seq libraries were prepared as previously described (Buenrostro et al., 2013). FACS-sorted cell populations (1×10^4 cells) were lysed and accessible chromatin was transposed using Nextera Tn5 transposase. Transposed DNA fragments were isolated using QIAGEN MinElute kit and amplified 5-10 cycles using Nextera PCR primers. ATAC-seq libraries were submitted for paired-end sequencing on Illumina HiSeq.

QUANTIFICATION AND STATISTICAL ANALYSIS

RNA Sequencing Analysis

FastQC (<https://www.bioinformatics.babraham.ac.uk/projects/fastqc/>) was used to assess sequencing quality. Reads were first mapped to the mouse genome using HiSat2 (Kim et al., 2015) (version 2.0.5). The genomic index along with the list of splice sites and exons were created by HiSat2 using the genome assembly GRCm38.p5 from ENSEMBL together with the comprehensive gene annotation for GRCm38.p5, Release M13, from GENCODE (Mudge and Harrow, 2015). Gene level counts were computed

using Rsubread (Liao et al., 2013) (options `isPairedEnd = TRUE`, `requireBothEndsMapped = TRUE`, `minOverlap = 80`, `countChimericFragments = FALSE`), and technical replicates were merged into single samples by summing the counts from each replicate. For the NK versus ILC analysis, genes were filtered out from further analysis if the mean read count across all samples containing both NK and ILC cells was less than 50. This resulted in 13,514 expressed genes that went into further analysis. DESeq2 (Love et al., 2014) was used to perform differential expression analysis on this set of genes. In order to find a common NK versus ILC1 signature across tissues while correcting for batch-specific effects across three batches of RNA-seq data, function `DESeq()` with default parameters was used to fit a full generalized linear model (\sim batch_B + batch_H + batch_J + organ + cell_type) (see Table S1). Each batch variable is a binary variable, where merged samples were assigned 1 in each column corresponding to the batch of each technical replicate; tissue (organ) factor is to model a tissue-specific variation in read counts for each gene. This approach allowed us to estimate a single value of RNA-seq $\log_2(\text{NK} / \text{ILC1})$ for each gene, along with a corresponding p value. Table S2 reports for each gene its average unnormalized “baseMean” read count across samples, $\log_2(\text{NK} / \text{ILC1})$ and the corresponding FDR-adjusted p value of significance, as well as RPKM value for expression in each sample. Differentially expressed genes were used for further analysis and visualization (Figures 2 and S2). 713 genes for Figure 2D were selected from the differential expression analysis if their FDR-adjusted p value was less than 10^{-5} ; 228 genes were selected for Figure S2B if their FDR-adjusted p value was less than 10^{-12} . Gene expression heatmaps in Figures 2 and S2 were generated with pheatmap (Kolde, R. pheatmap: <https://cran.r-project.org/web/packages/pheatmap/index.html>) using values $\log_{10}(\text{RPKM} + 1)$ that were Z-score normalized for each gene across all samples. Unsupervised hierarchical clustering was performed using hclust with Euclidean distance (method = “complete”) as implemented in pheatmap (Kolde). A subset of genes from a number of categories was manually selected for Figure 2E from the 713-gene signature set, averaging RPKM across biological replicates for each cell type. The estimated RNA-seq $\log_2(\text{NK} / \text{ILC1})$ values from this analysis were plotted for the core innate lymphoid cell class 1 (ILC1) and conventional natural killer cell (cNK) signature genes defined by Robinette et al. (2015) (as obtained from their Table S6) (Figure S2C). In order to compare the gene expression in PC CD49b⁻ Eomes⁻ cells with other cells in an unbiased manner (Figure S2A), and to determine if PC CD49b⁻ Eomes⁻ cells were closely associated with ILC1, we excluded PC CD49b⁻ Eomes⁻ samples and repeated all the analysis as described above, resulting in 847 genes detected as differentially expressed (FDR-adjusted $p < 10^{-5}$), including 405 genes with significantly higher expression in NK than in ILC1 (NK-specific) and 442 genes with significantly higher expression in ILC1 than in NK (ILC1-specific). We then estimated the RNA-seq $\log_2(\text{PC CD49b}^+ \text{Eomes}^+ / \text{CD49b}^- \text{Eomes}^-)$ values for all genes, using only the PC CD49b⁺ Eomes⁺ and CD49b⁻ Eomes⁻ samples. These values tended to be significantly larger for NK-specific genes than for all genes ($p < 2e-16$, Kolmogorov-Smirnov test) and tended to be significantly lower for ILC1-specific genes than for all genes ($p < 2e-16$), see Figure S2A. This suggested that PC CD49b⁻ Eomes⁻ samples had expression signature of ILC1 and further justified our labeling of them as ILC1 in the above analysis. All analysis starting from count table generation was conducted in the R statistical environment (version 3.2.4).

ATAC analysis

Paired-end reads were mapped to *Mus musculus* genome (mm10 assembly) using Bowtie2 (v 2.2.9) keeping only concordantly aligned paired mates. Tags per million were calculated as the total number of read counts overlapping 50-bin windows across either a 3kb or a 5kb window, centered around the transcriptional start site, divided by the total number of sequencing reads and multiplied by one million.

Statistical analyses

For graphs, data are shown as mean \pm SEM, and unless otherwise indicated, statistical differences were evaluated using a two-tailed unpaired Student's t test, assuming equal sample variance. Statistical differences in survival were determined by Gehan-Breslow-Wilcoxon Test analysis. $p < 0.05$ was considered significant. Graphs were produced and statistical analyses were performed using GraphPad Prism.

DATA AVAILABILITY

The datasets generated and analyzed during the current study will promptly be uploaded to a publicly available data repository.

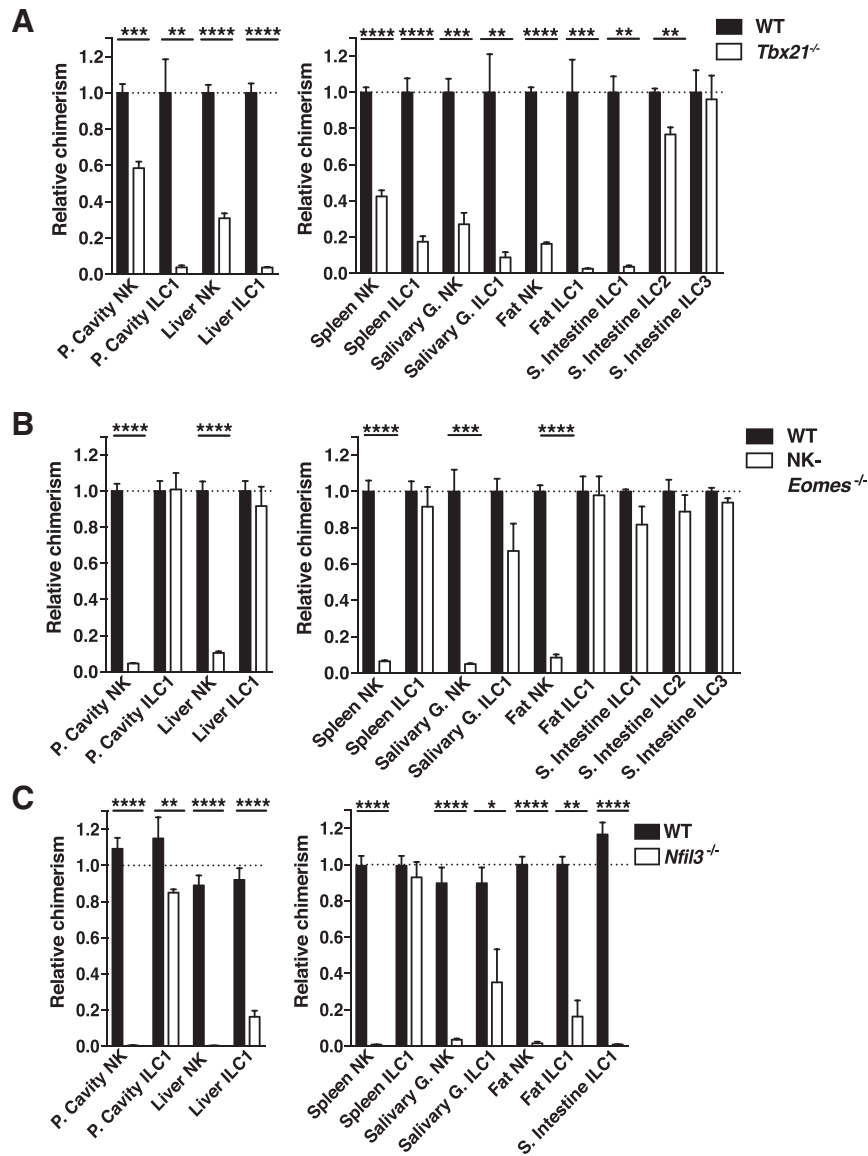


Figure S1. Peripheral Group 1 ILCs Have Differential Developmental Requirements for *Tbx21*, *Eomes*, and *Nfil3*, Related to Figure 2

(A-C) Mixed bone marrow chimeric (mBMC) mice harboring WT (CD45.1⁺) and selected transcription factor deficient (CD45.2⁺) bone marrow were analyzed 8 weeks post reconstitution for ILC populations. Data are shown as relative chimerism of the KO (CD45.2⁺) to WT (CD45.1⁺) ratio of lymphocyte populations normalized to the ratio of control WT (CD45.1⁺) and WT (CD45.2⁺) reconstituted mBMC. Quantification of relative chimerism of (A) WT and *Tbx21*^{-/-} mice, (B) WT and NK-*Eomes*^{-/-} mice, and (C) WT and *Nfil3*^{-/-} mice, in indicated peripheral organs. Data are representative of 2 independent experiments with n = 3-5 mice per group. Samples were compared using an unpaired, two-tailed Student's t test, and data are presented as the mean ± SEM (*p < 0.05, **p < 0.01, ***p < 0.001, ****p < 0.0001).

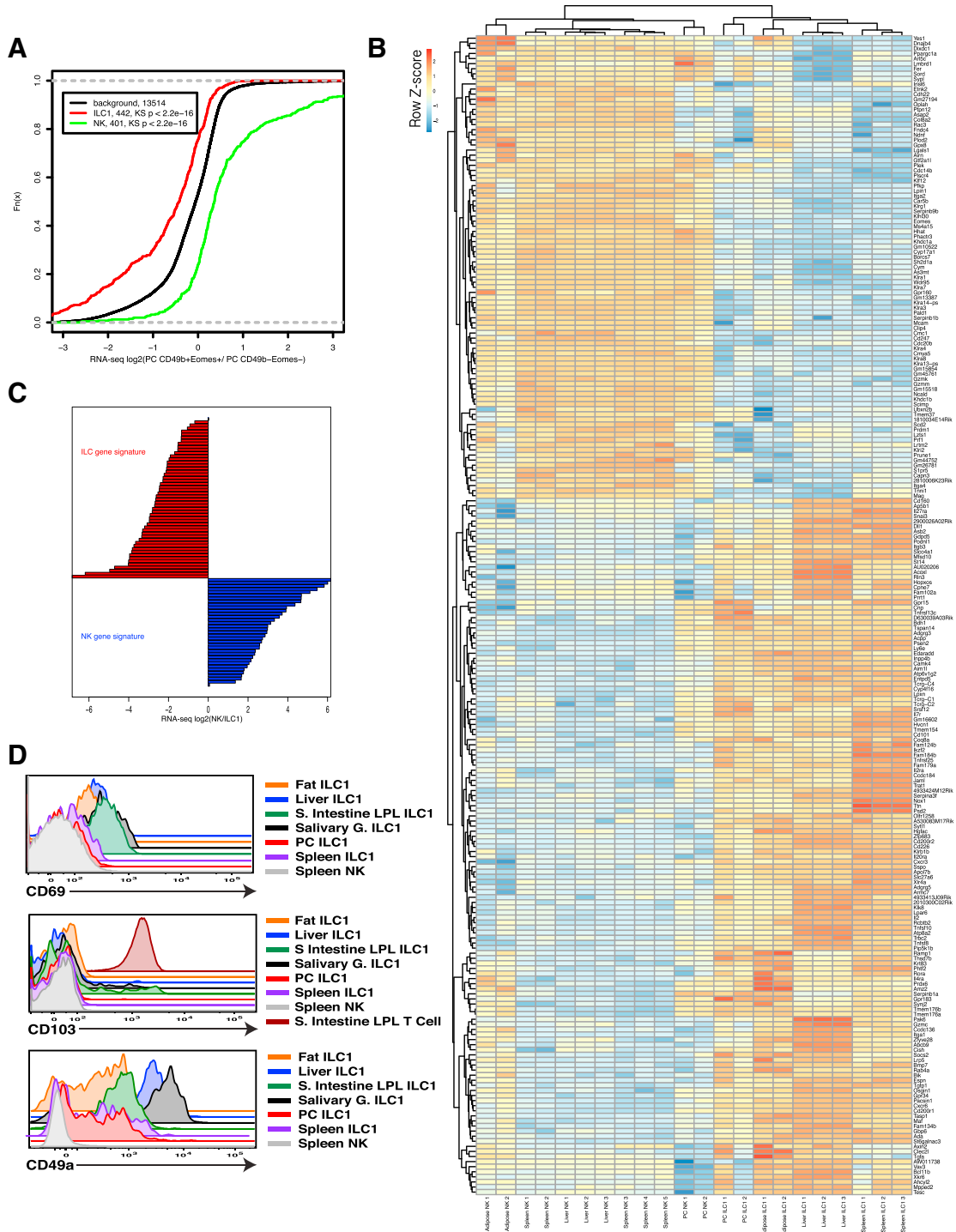


Figure S2. ILC1 Are a Transcriptionally and Phenotypically Distinct Lineage from NK during Homeostasis, Related to Figure 2
(A) CDF plot for comparison of RNA-seq log₂(PC CD49b⁺Eomes⁺ / PC CD49b⁻Eomes⁻) for all expressed genes with ILC1-specific and NK-specific genes identified from all other ILC1 and NK samples across tissues. Shown are the number of genes in each group, p value from the Kolomogorov-Smirnov test (see STAR Methods). (B) RNA-sequencing reveals gene expression signature of the indicated cell populations sorted purified from *Eomes*-GFP mice. Differentially expressed genes with FDR-adjusted p value less than 10⁻¹² (228 total). (C) RNA-seq log₂(NK / ILC1) for previously identified NK & ILC1 signature genes (see STAR Methods). (D) Representative histograms show indicated surface markers on resting NK and ILC1 in indicated tissue of WT mice. Data are representative of 2 - 3 independent experiments with (A-C) n = 40-50 mice, (D), n = 5 mice per group.

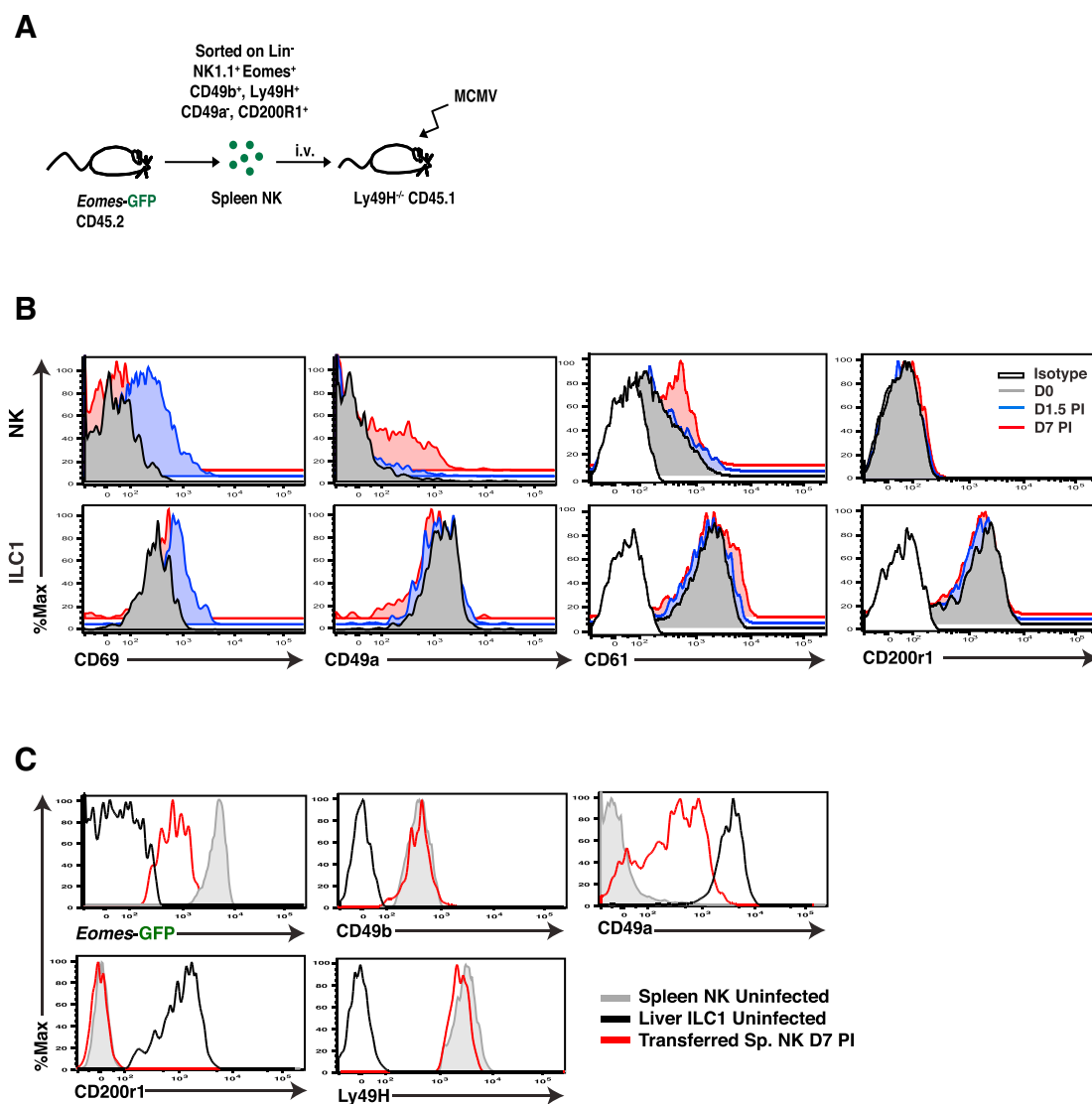


Figure S3. Phenotypic and Functional Stability of NK Cells during Viral-Induced Inflammation, Related to Figure 3

(A) Schematic of experiment. Briefly splenic NK cells (CD45.2⁺Lin⁻NK1.1⁺Eomes⁺CD49b⁺Ly49h⁺CD49a⁺CD200r1⁺) were sort purified from *Eomes-GFP* mice and adoptively transferred i.v. into Ly49H-deficient CD45.1⁺ recipients. Mice were then infected with MCMV i.p. (B) Representative histograms show indicated surface markers on NK and ILC1 harvested at indicated time points PI. (C) Representative histograms of indicated surface markers on uninfected splenic mNK (gray) and Liver ILC1 (black) and adoptively transferred splenic NK cells (red) recovered in the spleen seven days PI. Data are representative of 2 independent experiments with n = 3-5 mice per group.

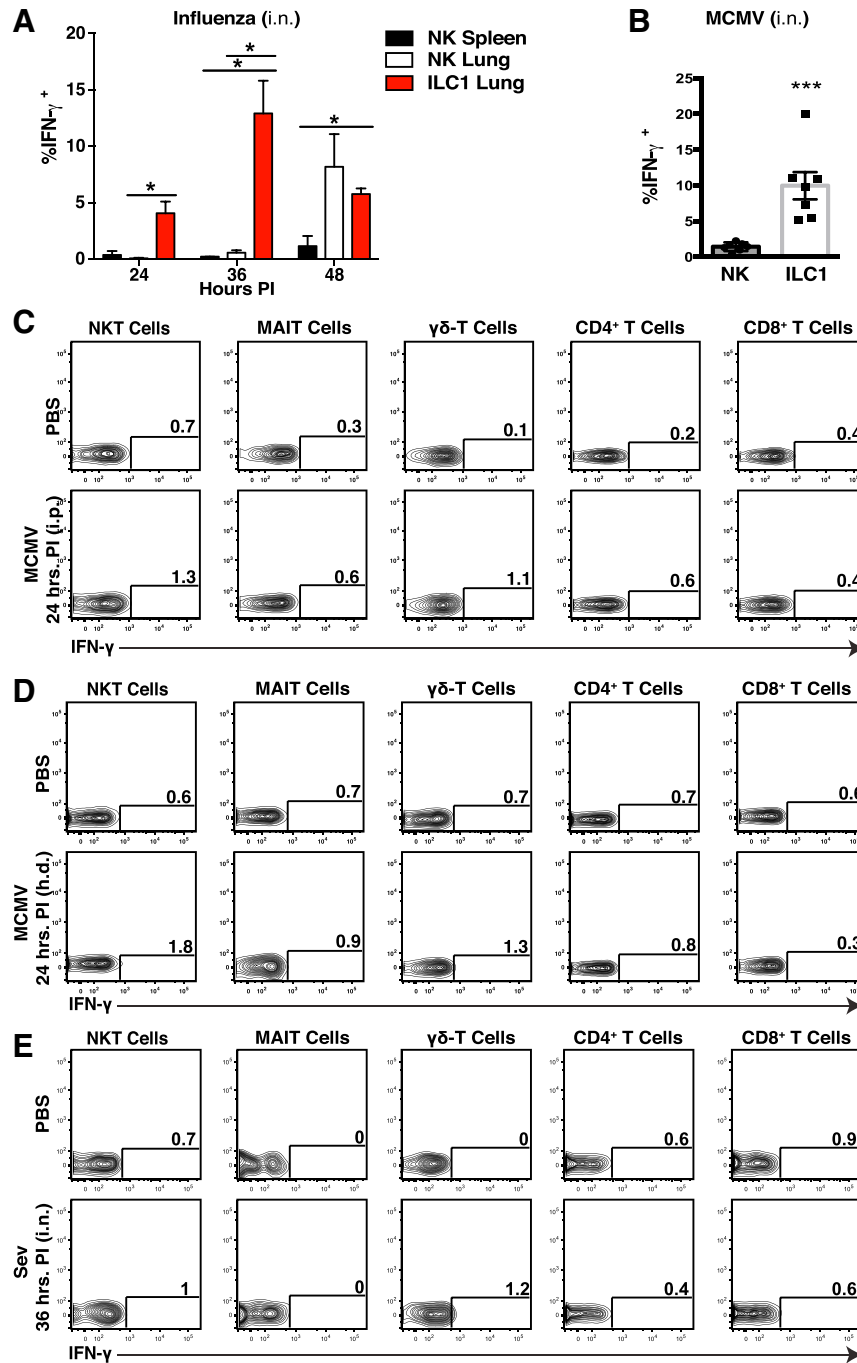


Figure S4. ILC1 Rapidly Produce IFN-γ Early during Host Anti-viral Response at Initial Sites of Infection, Related to Figure 4

(A and B) Quantification of intracellular IFN-γ staining of indicated group 1 ILC populations at various time points following either Influenza (i.n.) or MCMV (i.n.) in i.v. unlabeled fraction of indicated organ. (C-D) Flow plots show intracellular IFN-γ staining of indicated lymphocyte population from WT mice in PC (i.p. infection) or liver (h.d. infection) at 24 hr PI with MCMV. (E) Flow plots show intracellular IFN-γ staining of indicated lymphocyte population from WT mice in i.v. unlabeled fraction of the lung at 36 hr PI with Sev (i.n.) Data are representative of 2-3 independent experiments with n = 4-6 mice per group. Samples were compared using an unpaired, two-tailed Student's t test, and data are presented as the mean ± SEM (*p < 0.05, ***p < 0.001).

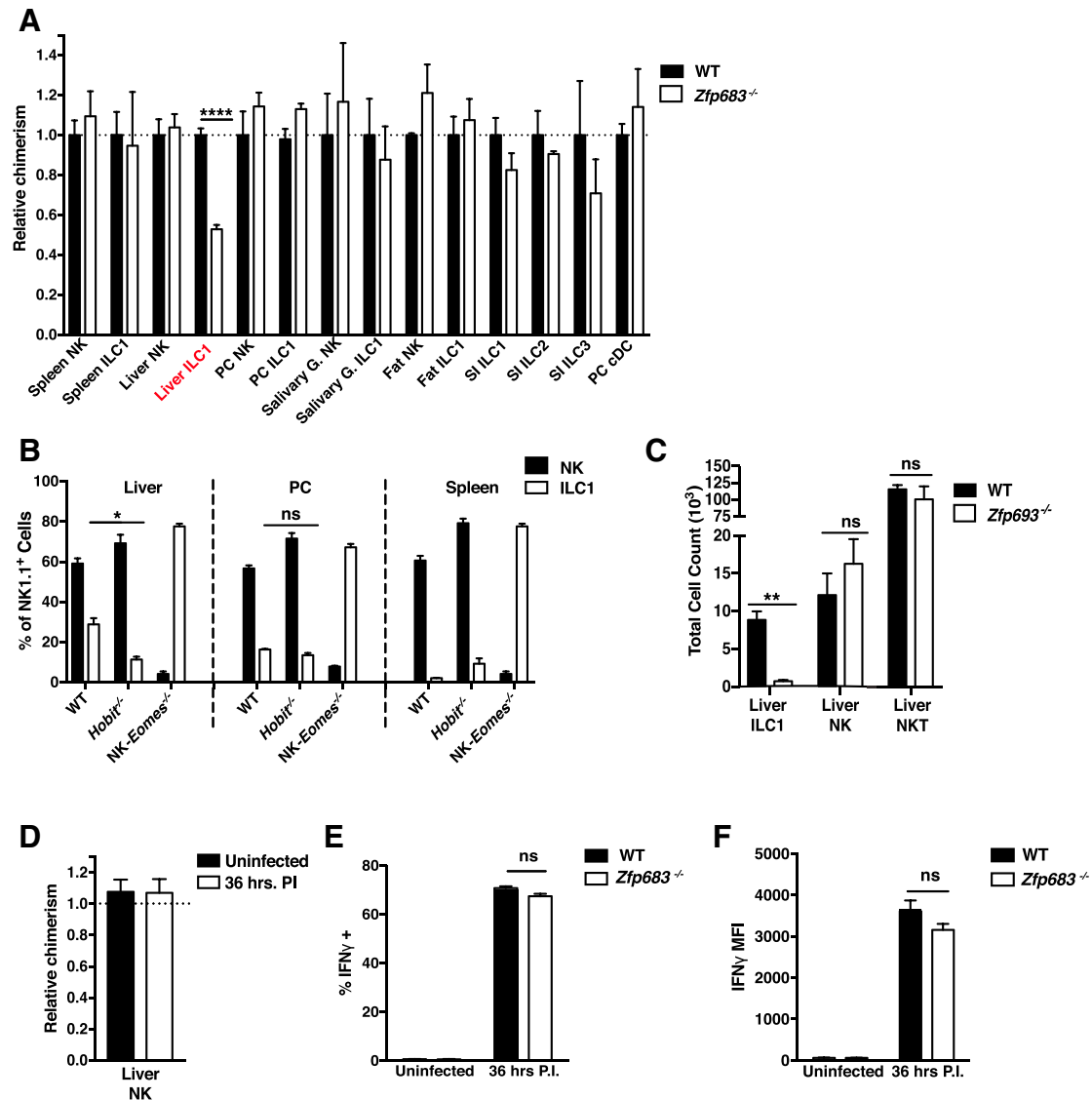


Figure S5. Peripheral Group 1 ILCs Have Differential Developmental Requirements for *Zfp683*, Related to Figure 5

(A) mBMC harboring WT (CD45.1⁺) and *Hobit*-deficient (*Zfp683*^{-/-}) (CD45.2⁺) bone marrow were analyzed 8 weeks post reconstitution for ILC populations. Data are shown as relative chimerism of the KO (CD45.2⁺) to WT (CD45.1⁺) ratio of lymphocyte populations normalized to the ratio of control WT (CD45.1⁺) and WT (CD45.2⁺) reconstituted mBMC. (B) Percent ILC1 and NK cells of total NK1.1⁺ cells in the PC, liver, and spleen of WT, *Zfp683*^{-/-}, and *NK-Eomes*^{-/-} mice. (C) The total cell number of indicated population WT and *Zfp683*^{-/-} mice (D-F) WT/*Zfp683*^{-/-} mBMC were infected with MCMV i.p. and analyzed in the liver at 36 hr PI. (D) Relative chimerism of *Zfp683*^{-/-} NK cells in the liver during infection. (E-F) Quantification of intracellular IFN- γ staining of NK cells by percentage and MFI. Data are representative of 2 independent experiments with n = 3-5 mice per group. Samples were compared using an unpaired, two-tailed Student's t test, and data are presented as the mean \pm SEM (*p < 0.05, **p < 0.01).

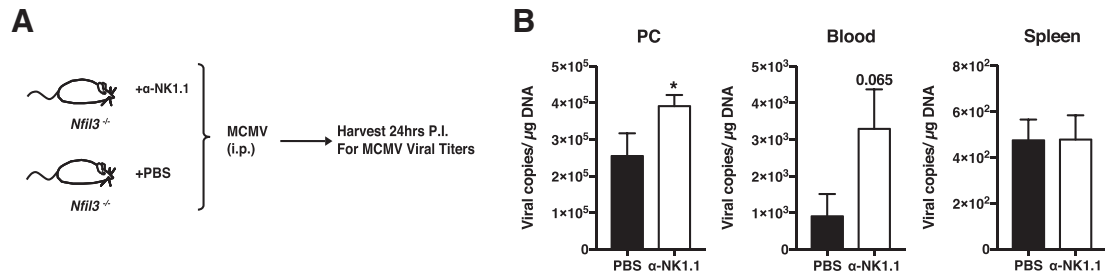


Figure S6. ILC1 Are Necessary to Confer Immediate Early Host Anti-viral Protection during MCMV Viral Challenge, Related to Figure 5
 (A and B) (A) Schematic of experiment. Briefly, *Nfil3*^{-/-} mice were treated with either PBS+ α -Ly49H or α -NK1.1+ α -Ly49H and then infected with MCMV i.p. (B) Viral titers of each indicated cohort are shown for PC, Blood, and Spleen at 24 hr PI. Data are representative of 2 independent experiments with n = 3-5 mice per group. Samples were compared using an unpaired, two tailed Student's t test, and data are presented as the mean \pm SEM (*p < 0.05)

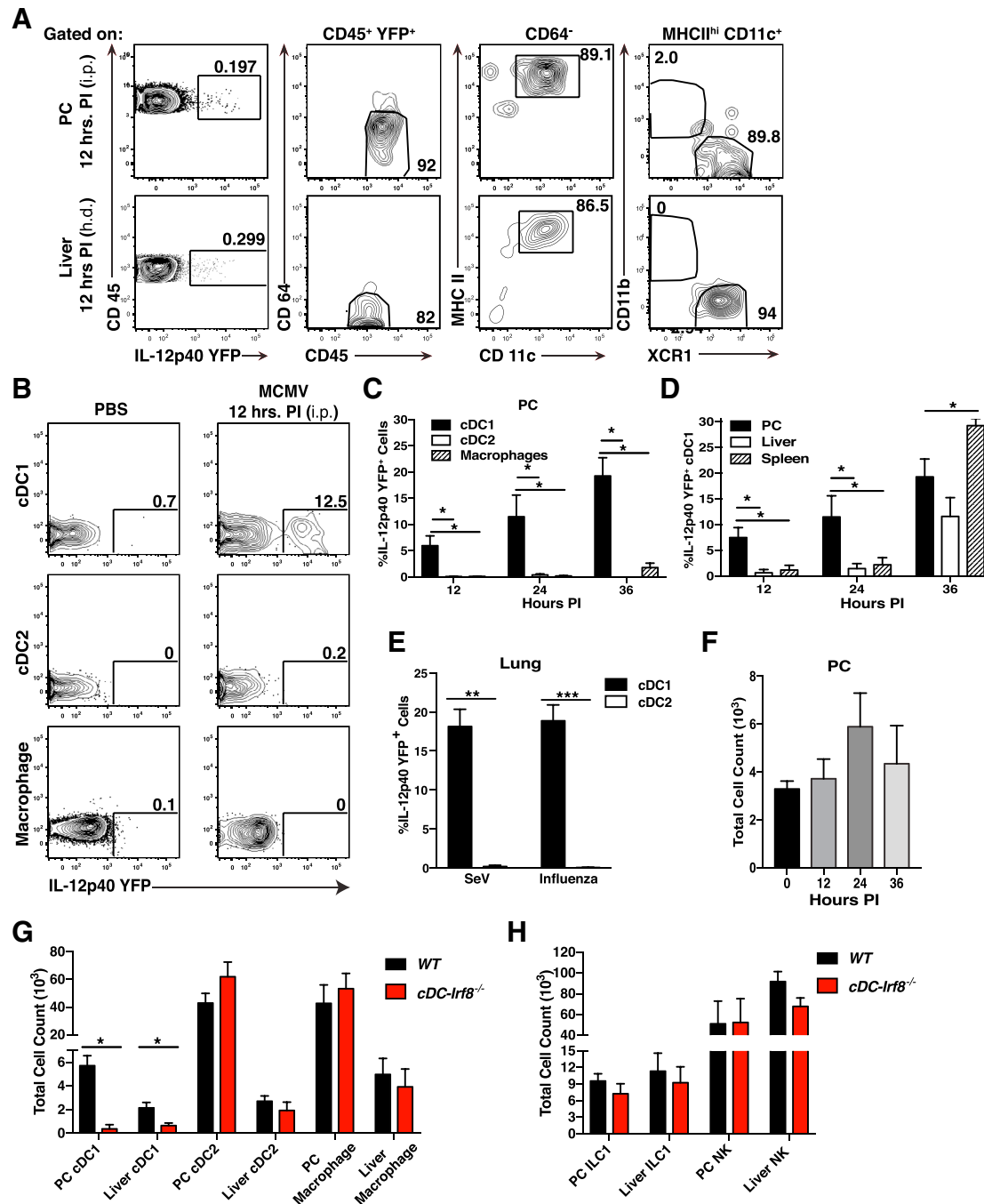


Figure S7. Tissue-Resident cDC1 Are the Main Producers of IL-12 Early in Initial MCMV-Infected Tissues and Are Required for Optimal IFN- γ Production by ILC1, Related to Figure 6

(A-E) *Il-12p40*-YFP mice were infected with MCMV by either i.p. or h.d. injection and peripheral tissues were harvested and analyzed for YFP⁺ cells at various time points PI. (A) Representative plots of non-biased analysis of YFP⁺ cells in PC (i.p. infection, upper panel) and liver (h.d. infection lower panel,) at 12 hr PI (B-C) (B) Flow plots and (C) graphs show percentages of YFP⁺ cells in different PC populations at 12, 24, and 36 hr PI (i.p.). (D) Quantification of YFP⁺ cDC1 in peripheral tissues at 12, 24, and 36 hr PI (i.p.). (E) Quantification of YFP⁺ in the lung 36 hr PI with SeV or Influenza (i.n.). (F) The total cell number of cDC1 in the PC at 12, 24, and 36 hr PI (i.p.). (G-H) Peripheral tissue of cDC-WT and cDC-*Irf8*^{-/-} mice were harvested and analyzed for total cell count in indicated populations. Data are representative of 2 independent experiments with n = 3-5 mice per group. Samples were compared using an unpaired, two-tailed Student's t test, and data are presented as the mean \pm SEM (*p < 0.05).